Astronomy & Astrophysics manuscript no.
(will be inserted by hand later)

AGN and starburst radio activity in the A3558 cluster complex

S. Giacintucci[1], T. Venturi[2], S. Bardelli[1], D. Dallacasa[2,3], and E. Zucca[1]

[1] INAF - Osservatorio Astronomico di Bologna, via Ranzani 1, I–40127 Bologna, Italy
[2] Istituto di Radioastronomia del CNR, via Gobetti 101, I-40129, Bologna, Italy
[3] Dipartimento di Astronomia, Università di Bologna, via Ranzani 1, I–40127, Bologna, Italy

Received 00 - 00 - 0000; accepted 00 - 00 - 0000

Abstract. In this paper we present Very Large Array (VLA) 1.4 GHz (21 cm) observations of the region between the centres of A3558 and A3562, in the major cluster merger complex of the Shapley Concentration. Our final catalogue includes a total of 174 radio sources above the flux density limit of 0.25 mJy b^{-1}. By cross-correlation with optical and spectroscopic catalogues we found 33 optical counterparts belonging to the Shapley Concentration.
We investigated the effects of cluster merger on the radio emission properties of the galaxy population by means of the radio source counts and the radio luminosity functions (RLF). We found that the radio source counts are consistent with the field source counts. The RLF of elliptical and S0 galaxies in the region surveyed here, is consistent with the "universal" RLF for early–type galaxies. This result suggests that the deficit in radio galaxies found in our previous works over the whole A3558 chain, is entirely due to the cluster A3558. A population of faint radio galaxies ($\log P_{1.4\ GHz}$(W Hz^{-1}) $\lesssim$22) is also found. Half of these objects are also blue, suggesting that starburst is the main mechanism driving the radio emission. Finally, we detected 14 spiral radio galaxies, whose ratio between radio and optical emission is similar to those found in galaxies located in rich and dynamically evolved clusters.
Our results are briefly discussed in the light of the age and stage of the merger in the A3558 cluster complex.

Key words. radio continuum: galaxies - galaxies: clusters: general - galaxies: clusters: individual: A3562 - galaxies: clusters: individual: SC 1329−313 - galaxies: clusters: individual: SC 1327−312.

1. Introduction

Evidence is accumulating that the interaction processes between clusters of galaxies, known as cluster mergers, may significantly affect the radio emission characteristics of the cluster galaxy population. In particular, the evolution of galaxies and the properties of their nuclear and/or star forming activity are undoubtely influenced by the interaction with the environment. In this frame, cluster merging and group accretion seem to play an important role, but it is not yet completely understood how the merging environment affects the nuclear and starburst emission in galaxies. Owen et al. (1999) suggested that merging may trigger the radio emission, both in the form of nuclear activity and starburst phenomena. Burns et al. (1994) interpreted the presence of post-starburst galaxies in the X–ray and radio bridge connecting the Coma cluster and the NGC 4839 group as consequence of a recent merging process between these two structures. Using numerical simulations, Bekki (1999) concluded that the tidal gravitational field of a cluster merger may drive a considerable transfer of gas to the central regions of galaxies, leading to enhanced star formation activity or feeding the central engine of active galactic nuclei. Vollmer et al. (2001) suggested that a local burst of star formation could be due to re-accretion of gas after a ram pressure stripping event, which is thought to be responsible for the HI deficit of spiral galaxies in the central regions of nearby clusters with respect to the field galaxies of the same morphological type and optical size (Gunn & Gott, 1972; Bothun & Dressler, 1986). On the other hand, Fujita et al. (1999) and Balogh et al. (1998) claimed that gas stripping resulting from ram pressure is important in preventing gas supply to the central regions of the galaxies and may suppress star formation. Finally Venturi et al. (2000, hereinafter V2000) found evidence that merging may anticorrelate with the radio emission, possibly switching off previously existing radio galaxies, or temporarily inhibiting the nuclear radio activity.
A major problem in our current knowledge of the role of cluster mergers on the radio emission and in the interpretation of the observations is the lack of statistics. Only few clusters of galaxies were deeply imaged over their whole extent (i.e. A2125, Dwarakanath & Owen, 1999; A2255, Miller & Owen, 2003 (hereinafter MO03); A2256, Miller et al., 2003; A2645, Owen et al., 1999; the Shapley supercluster chains A3528, A3558 and A3571, Venturi et al.

2001, 2000 and 2002 respectively), and the complexity of the phenomenon clearly needs a much larger observational support. Cluster mergers evolve over a timescale of $\sim$ Gyr, while typical ages of radio sources are of the order of few times 10^7 – 10^8 years, therefore it is of crucial importance to identify the effects of the various stages of a merger event. For this reason it is essential to carry out deep radio observations of a large number of galaxy clusters, at different merger stages.

In order to study the effects of a major cluster merger event after the first core–core encounter on the nuclear and starburst radio emission, in this paper we present 1.4 GHz Very Large Array (VLA) observations of the cluster A3562 and the poor groups SC 1329−313 and SC 1327−312, at the eastern side of the A3558 cluster complex. In the following we will refer to the area surveyed as A3558–C. This work is part of a larger project which aims to study the influence of the ongoing merger in the core of the Shapley Concentration on the radio/optical properties of the cluster galaxies, both from a statistical point of view and through a detailed analysis of the physical properties of the extended radio galaxies. In section 2 we briefly overview the optical and X–ray properties of A3558–C, with emphasis on the cluster A3562 and on the poor groups SC 1329−313 and SC 1327−312; the observations and data reduction are presented in Section 3; in Section 4 we present the 1.4 GHz radio sample and the source counts; in Section 5 we deal with the optical identifications and in Section 6 we present the general properties of the radio galaxies in this region; the results of the analysis of the radio luminosity function (RLF) for the early-type and late-type galaxy populations are given in Section 7; discussion and conclusions are given in Section 8.

We assume $H_0 = 100$ km s^{-1} Mpc^{-1} and q_o=0.5. If we define h=H$_o$/100, at the average redshift of the Shapley Concentration ($z = 0.05$) this leads to a linear scale of 1 arcsec = 0.67 h^{-1} kpc. We will assume $S \propto \nu^{-\alpha}$.

2. The cluster merger in A3558–C

The dynamical centre of the Shapley Supercluster can be identified with the A3558 cluster complex, a chain of interacting clusters located at a mean redshift $z = 0.0483$ and spanning ~ 7.5 h^{-1} Mpc (projected), almost orthogonal to the line of sight. The chain is formed by the three ACO (Abell et al. 1989) clusters A3558, A3562 and A3556, and includes the two poor groups SC 1327−312 and SC 1329−313 (Figure 1).

The A3358 cluster complex has been extensively studied over a wide range of bands, from radio wavelengths up to X–ray energies, and the physical connection and the merging stage of all clusters in this region is suggested by observational data in the radio (V2000, Venturi et al. 2003, hereinafter V2003), optical (Bardelli et al. 1994) and X–ray bands (Bardelli et al. 1996, Ettori et al. 1997).

The distribution of the hot gas in this region remarkably follows the distribution of the optical galaxies, and a detailed substructure analysis carried out by Bardelli et al. (1998a) revealed that the whole structure is characterized by a large number of subcondensations, further evidence of its dynamical activity. In addition, the galaxy distribution in the A3558 chain resembles the results of the numerical simulations carried out by Roettiger et al. (1997) for the case of a collision of two clusters. The observational scenario suggests that the whole region is the result of a major merger with the cluster A3558, seen after the first core–core encounter (Bardelli et al. 1998b, 2002). In this frame, all that visible in the chain beyond A3558 itself, i.e. A3556, A3562 and the two small groups SC 1327−312 and SC 1329−313, would be the remains of the colliding cluster (see Fig. 1). In the region between A3558 and A3562, where the initial position of the merger shock is expected, Bardelli et al. (1998b) found an enhanced fraction of blue galaxies.

The whole A3558 cluster complex was surveyed at 22/13 cm with the Australia Telescope Compact Array (ATCA, Venturi et al. 1997, Venturi et al. 1998, V2000) and a number of interesting results emerged from the radio analysis. In particular, the outskirts of the chain, i.e. A3556 and A3562, contain the largest number of cluster radio sources and the four extended radio galaxies. Moreover, the radio luminosity function computed for elliptical galaxies over the whole complex is considerably lower that the "universal" radio luminosity function for ellipticals derived by Ledlow and Owen (1996, hereinafter LO96), suggesting a possible connection with the cluster merger in this region. Finally, a cluster radio halo was detected at the centre of A3562 (V2000, V2003), as a further evidence of the role of merger on the cluster radio emission.

The properties of A3562, SC 1327-312 and SC 1329−313 are summarised in Table 1, where we report:
− columns 2 and 3: J2000 coordinates;
− columns 4 and 5: Bautz-Morgan type and richness;
− columns 6 and 7: mean heliocentric velocity and velocity dispersion;
− column 8 and 9: X–ray temperature and luminosity.

3. Observations and Data Reduction

The 1.4 GHz (21 cm) observations of A3562 and of the two SC groups 1327−312 and 1329−313 were carried out on 10 July 2000 with the Very Large Array (VLA), operating in the DnC configuration. The observations were carried out in continuum mode with a 50 MHz bandwidth, for a total duration of 4 hours. We switched among the four fields every 4.5 minutes. 3C286 was used as primary calibrator, and 1316−336 as phase calibrator. The logs of the observations are given in Table 2.

The region of interest was covered with four different pointings; the resolution is $41.98'' \times 35.13''$ at the declination of the A3558 complex.

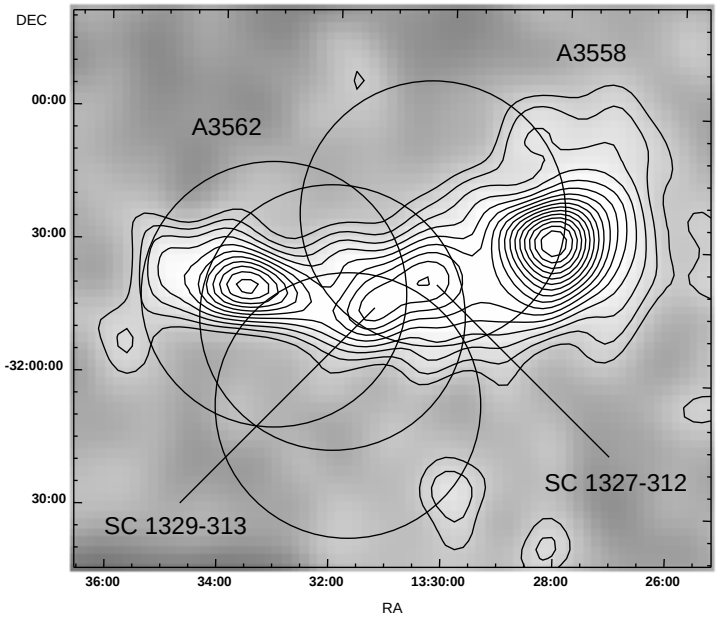

Fig. 1. Grey scale and isocontours of the galaxy density to $b_J = 19.5$ in A3558–C from the COSMOS catalogue. The cluster A3556, located westward of A3558, is not included in the figure. The centres of the superposed circles correspond to the pointing centres of the observations. The radius of each circle is 30 arcmin (i.e. primary beam size of the VLA at 1.4 GHz).

Table 1. Cluster properties

Cluster	RA_{J2000}	DEC_{J2000}	B–M	R	$< v >$ km s^{-1}	σ_v km s^{-1}	kT keV	L_X (2–10 keV) h^{-2} erg s^{-1}
(1)	(2)	(3)	(4)	(5)	(6)	(7)	(8)	(9)
SC 1327−312	13 29 47	−31 36 29	–	–	14844^{+105}_{-211} (a)	691^{+158}_{-146} (a)	$4.11^{+0.43}_{-0.36}$ (c)	3.76×10^{43} (c)
SC 1329−313	13 31 36	−31 48 46	–	–	(T520) 13280^{+80}_{-95} (b) (T496) 14690^{-101}_{-99} (b)	482^{+87}_{-49} (b) 537^{+87}_{-32} (b)	$3.49^{+0.27}_{-0.24}$ (c)	2.36×10^{43} (c)
A3562	13 33 30	−31 40 00	I	2	14492^{+225}_{-286} (a)	913^{189}_{-96} (a)	$5.13^{+0.21}_{-0.19}$ (d)	5.25×10^{43} (d)

Notes to Table 1. The coordinates of the centre for A3562 are taken from Abell et al. (1989), the coordinates for SC 1327–312 are from Bardelli et al. (1996) and for SC 1329–313 from Breen et al. (1994). Note that the SC 1329 group has a bimodal velocity distribution: the optical clumps associated to the two velocity peaks are named T520 and T496 (Bardelli et al., 1998a). (a) Bardelli et al. (1998b); (b) Bardelli et al. (1998a); (c) Bardelli et al. (2002); (d) Ettori et al. (2000).

The observations were carried out using the mosaicing facility of the VLA. Pointing # 1 and # 2 were chosen to be centered respectively on the head-tail J1333−3141 in the centre of A3562, where the radio halo lies, and on the diffuse radio source J1332−3146a in the region between A3562 and the SC 1329−313 group (V2000). The remaining pointings were chosen in order to remove the sidelobes from the confusing sources at the field edges and to ensure uniform sensitivity over the whole region between the centre of A3562 and the SC groups.

The data reduction was carried out using the standard procedure (calibration, Fourier inversion, clean and restore) of the NRAO AIPS (Astronomical Image Processing System) package. We reduced the data and imaged each field separately. The final images were then mosaiced (i.e. linearly combined) using the AIPS task LTESS. The average noise in the individual final images is ∼0.50

Table 2. Logs of the Observations

Field # (1)	RA_{J2000} (2)	DEC_{J2000} (3)	Array (4)	Int. Time (h) (5)	rms (1.4 GHz) mJy/b (6)
1	13 33 32	−31 40 60	DnC	1	0.05
2	13 32 02	−31 46 60	DnC	1	0.05
3	13 30 19	−31 22 57	DnC	1	0.05
4	13 31 43	−32 06 45	DnC	1	0.05

μJy b^{-1} in all four fields. We assume as reliable all detections with flux density peak $S_{1.4GHz} \geq$0.25 mJy b^{-1}, corresponding to 5σ confidence level. Such limit implies a limit on radio power of $\log P_{1.4GHz}$ (W Hz^{-1}) = 20.83 at the average distance of A3558–C. We note that our detection limit is near the confusion limit at the frequency and resolution of the images presented here. In order to evaluate this effect, we cross–checked our detections on a pure uniform weight image, where the confusion is considerably lower, ad considered as reliable detections only those sources passing the cross-check.

4. The sample of radio sources

We detected a total of 174 radio sources at 1.4 GHz above the peak flux density limit of 0.25 mJy b^{-1}. The source list is reported in Table 3, where we give:
− columns 1, 2 and 3: name (VLA–) and J2000 position;
− column 4: flux density at 1.4 GHz corrected for the primary beam attenuation. The values were derived with task JMFIT for unresolved or marginally resolved sources, while they were obtained by means of TVSTAT for the extended sources;
− column 5: radio morphology. We classified the sources as unres. = unresolved and ext. = extended. Moreover we note that D = double and HT = head–tail. For the double source we give the position of the radio barycentre and for the extended sources we give the position of the radio peak.

As clear from Table 3 most of the radio sources detected at 1.4 GHz are unresolved; only 23 radio sources are extended, i.e. 13% of the total.

Our observations confirm the presence of a radio halo at the centre of A3562 (not listed in Table 3), encompassing the head–tail radio galaxy J1333−3141. The halo has a flux density of $S_{1.4GHz} = 20$ mJy, a low surface brightness ($\leq$ 0.175 mJy b^{-1}) and an irregular shape, with largest angular size of $\sim 8'$. The properties and the origin of this source are discussed in a different paper (V2003).

We note that the region presented in this paper (A3558–C) partly overlaps with the area covered in the ATCA survey presented in V2000. We carefully checked all sources in the common region, and found that all differences can be accounted for either by the different u–v coverage, resolution and/or sensitivity of the two sets of observations. Due to the different resolutions ($\sim 10'' \times 5''$ for the ATCA observations), in a number of cases the radio emission detected with the present observations is actually a blend of two or more sources in the ATCA 22 cm sample.Those cases of source blending relevant to the discussion of this paper are briefly commented in the Appendix.

4.1. Radio source counts

We computed the source counts for our radio sample in A3558–C, in order to test if the optical galaxy overdensity and the ongoing merging scenario proposed here reflect into a higher number of radio sources with respect to the field radio sources counts.

Since the sensitivity in the final images of the four fields covered by our observations is not uniform due to the VLA primary beam attenuation, the 1.4 GHz sample is not complete to the flux density limit of 0.25 mJy. For this analysis we therefore considered only the radio sources with $S_{1.4GHz} \geq 0.50$ mJy within a radius of 15.5 arcmin from the centre of each field. At such distance the primary beam attenuation of the VLA at 1.4 GHz is reduced by a factor of two, and sources with flux density $S_{1.4GHz} \geq$ 0.50 mJy are seen as sources with $S_{1.4GHz} \geq 0.25$ mJy before the correction. At the distance of A3558–C this limit implies a radio power $\log P_{1.4GHz}$(W Hz^{-1})= 21.13.

Our results are in very good agreement with the radio source field counts (Prandoni et al. 2001) and with the statistical analysis over the whole A3558 cluster chain carried out in V2000. This implies that even in an overdense and merging region such as the one considered here, the radio source counts are dominated by field sources, at least for $\log P_{1.4GHz}$ (W Hz^{-1}) $\gtrsim$21.

5. Optical Identifications

In order to find as many optical counterparts as possible, we cross–correlated the radio positions of all sources in our sample with four different optical catalogues. Our reference catalogue is the COSMOS/UKST Southern Sky Object Catalogue (Yentis et al. 1992), limited to b_J = 19.5; then for fainter magnitudes we considered also the SuperCOSMOS/USKT Southern Sky Object Catalogue (Hambly et al. 2001), the APM Catalogue (Maddox et

Table 3. Source list and flux density values

Name VLA−	RA_{J2000}	DEC_{J2000}	$S_{1.4GHz}$ (mJy)	Radio Morphology
J1328−3119	13 28 29.35	−31 19 14.7	66.34	unres.
J1328−3134	13 28 31.50	−31 34 50.4	126.80	unres.
J1328−3115	13 28 35.09	−31 15 22.1	1.97	unres.
J1329−3126	13 29 00.02	−31 26 26.0	81.92	ext.
J1329−3131	13 29 04.61	−31 31 02.1	86.80	unres.
J1329−3112	13 29 09.12	−31 12 56.8	5.37	unres.
J1329−3121	13 29 13.32	−31 21 51.1	23.65	unres.
J1329−3129a	13 29 29.43	−31 29 43.7	18.90	unres.
J1329−3100	13 29 31.67	−31 00 17.0	5.48	unres.
J1329−3116	13 29 31.88	−31 16 51.9	25.06	ext.
J1329−3102	13 29 39.15	−31 02 08.3	2.15	unres.
J1329−3119a	13 29 49.32	−31 19 37.3	6.02	unres.
J1329−3101	13 29 49.42	−31 01 44.6	3.03	unres.
J1329−3122	13 29 50.76	−31 22 55.6	22.43	ext.
J1329−3057	13 29 51.22	−30 57 47.2	65.38	unres.
J1329−3056	13 29 52.90	−30 56 00.7	123.04	ext. (D)
J1329−3119b	13 29 55.02	−31 19 57.7	4.53	unres.
J1329−3129b	13 29 55.32	−31 29 36.7	8.62	unres.
J1330−3124a	13 30 05.10	−31 24 36.3	6.89	unres.
J1330−3144a	13 30 05.20	−31 44 51.7	4.01	unres.
J1330−3113	13 30 05.59	−31 13 44.8	1.79	unres.
J1330−3215a	13 30 05.60	−32 15 54.3	1.81	unres.
J1330−3143a	13 30 05.82	−31 43 42.2	4.02	unres.
J1330−3102	13 30 07.17	−31 02 19.4	10.07	ext.
J1330−3103	13 30 08.55	−31 03 46.2	1.08	unres.
J1330−3144b	13 30 08.56	−31 44 02.8	3.26	unres.
J1330−3116	13 30 09.79	−31 16 10.8	2.68	unres.
J1330−3124b	13 30 10.06	−31 24 05.6	5.81	unres.
J1330−3214	13 30 14.71	−32 14 46.3	1.94	unres.
J1330−3122	13 30 19.06	−31 22 58.2	439.08	unres.
J1330−3159	13 30 19.41	−31 59 40.0	2.05	unres.
J1330−3201	13 30 21.69	−32 01 33.3	3.27	unres.
J1330−3129	13 30 30.79	−31 29 59.3	14.13	unres.
J1330−3153	13 30 33.03	−31 53 29.1	1.14	unres.
J1330−3152	13 30 39.44	−31 52 11.0	1.56	unres.
J1330−3105	13 30 40.88	−31 05 47.3	3.04	unres.
J1330−3215b	13 30 41.11	−32 15 21.4	0.65	unres.
J1330−3134	13 30 41.21	−31 34 17.4	3.86	ext.
J1330−3141	13 30 42.14	−31 41 35.7	4.18	unres.
J1330−3120	13 30 47.27	−31 20 30.4	2.22	unres.
J1330−3143b	13 30 47.95	−31 43 40.2	7.77	ext.
J1330−3148	13 30 48.03	−31 48 45.9	1.03	unres.
J1330−3226	13 30 48.11	−32 26 07.5	2.61	unres.
J1330−3145	13 30 48.27	−31 45 48.2	0.98	unres.
J1330−3146	13 30 51.97	−31 46 00.0	1.98	unres.
J1330−3209	13 30 52.00	−32 09 02.3	0.73	unres.
J1330−3127	13 30 52.33	−31 27 01.1	1.04	unres.
J1330−3204	13 30 55.62	−32 04 01.3	9.64	unres.
J1330−3208	13 30 59.20	−32 08 54.2	0.51	unres.
J1331−3144	13 31 00.60	−31 44 51.4	2.55	unres.
J1331−3140	13 31 01.87	−31 40 35.3	0.60	unres.
J1331−3127	13 31 05.38	−31 27 00.1	4.78	unres.
J1331−3154a	13 31 06.71	−31 54 59.9	8.48	ext.
J1331−3119	13 31 10.88	−31 19 27.6	14.52	unres.
J1331−3139	13 31 12.00	−31 39 27.1	9.48	unres.
J1331−3155a	13 31 14.14	−31 55 49.2	0.78	unres.

Table 3. Continued

Name VLA−	RA_{J2000}	DEC_{J2000}	$S_{1.4GHz}$ (mJy)	Radio Morphology
J1331−3124	13 31 14.63	−31 24 17.9	2.29	unres.
J1331−3101	13 31 15.08	−31 01 38.6	12.72	ext.
J1331−3135	13 31 16.85	−31 35 34.2	0.93	unres.
J1331−3128	13 31 16.91	−31 28 20.1	22.28	unres.
J1331−3113	13 31 18.79	−31 13 56.2	2.38	unres.
J1331−3143	13 31 19.88	−31 43 50.2	14.53	ext.
J1331−3108	13 31 25.72	−31 08 21.5	6.04	unres.
J1331−3149a	13 31 27.54	−31 49 14.7	1.32	unres.
J1331−3121a	13 31 29.66	−31 21 45.4	12.93	unres.
J1331−3209a	13 31 31.57	−32 09 27.4	1.06	ext.
J1331−3133a	13 31 37.66	−31 33 08.4	3.69	unres.
J1331−3121b	13 31 39.06	−31 21 59.7	4.85	ext.
J1331−3154b	13 31 39.29	−31 54 15.6	2.04	ext.
J1331−3209b	13 31 41.58	−32 09 43.8	0.68	unres.
J1331−3147a	13 31 41.96	−31 47 17.7	0.47	unres.
J1331−3206	13 31 42.95	−32 06 38.2	129.85	unres.
J1331−3147b	13 31 42.98	−31 47 45.8	0.47	unres.
J1331−3221	13 31 43.37	−32 21 36.2	16.39	ext.
J1331−3132	13 31 44.04	−31 32 52.5	1.34	unres.
J1331−3116a	13 31 48.62	−31 16 23.8	51.46	unres.
J1331−3133b	13 31 48.63	−31 33 07.8	1.04	unres.
J1331−3148	13 31 50.22	−31 48 47.4	1.32	unres.
J1331−3142	13 31 50.89	−31 42 49.7	2.13	unres.
J1331−3155b	13 31 53.27	−31 55 33.4	2.06	unres.
J1331−3116b	13 31 54.18	−31 16 44.6	8.74	unres.
J1331−3154c	13 31 54.83	−31 54 01.2	1.19	unres.
J1331−3149b	13 31 59.47	−31 49 19.8	1.82	ext.
J1332−3136a	13 32 00.29	−31 36 26.4	0.40	unres.
J1332−3112	13 32 02.35	−31 12 44.8	4.53	unres.
J1332−3146a	13 32 02.78	−31 46 50.0	15.11	ext.
J1332−3152a	13 32 05.13	−31 52 30.4	0.49	unres.
J1332−3141a	13 32 05.34	−31 41 23.4	11.32	unres.
J1332−3228	13 32 11.04	−32 28 23.7	11.17	unres.
J1332−3123a	13 32 14.42	−31 23 59.8	3.02	unres.
J1332−3131a	13 32 15.98	−31 31 25.7	0.83	unres.
J1332−3152b	13 32 17.52	−31 52 49.6	15.78	unres.
J1332−3123b	13 32 27.65	−31 23 49.5	21.09	unres.
J1332−3151	13 32 29.84	−31 51 01.8	0.86	unres.
J1332−3141b	13 32 31.71	−31 41 54.5	3.24	unres.
J1332−3131b	13 32 35.38	−31 31 41.8	1.79	unres.
J1332−3135	13 32 37.56	−31 35 55.5	0.76	unres.
J1332−3201	13 32 40.51	−32 01 56.9	32.19	ext.
J1332−3124	13 32 42.47	−31 24 52.4	0.96	unres.
J1332−3155	13 32 43.25	−31 55 11.0	0.58	unres.
J1332−3146b	13 32 43.92	−31 46 53.2	1.41	unres.
J1332−3142a	13 32 44.59	−31 42 44.8	0.34	unres.
J1332−3158	13 32 44.98	−31 58 24.7	17.64	unres.
J1332−3136b	13 32 46.59	−31 36 58.5	1.92	unres.
J1332−3156	13 32 50.23	−31 56 11.5	0.76	unres.
J1332−3142b	13 32 51.48	−31 42 37.3	0.40	unres.
J1332−3144	13 32 55.07	−31 44 14.4	0.90	unres.
J1332−3128	13 32 55.69	−31 28 12.3	1.12	unres.
J1332−3134	13 32 56.48	−31 34 52.5	0.72	unres.
J1332−3146c	13 32 57.03	−31 46 09.4	0.47	unres.
J1332−3123c	13 32 57.21	−31 23 53.2	6.56	unres.
J1332−3148	13 32 57.58	−31 48 04.2	2.41	unres.

Table 3. Continued

Name VLA−	RA_{J2000}	DEC_{J2000}	$S_{1.4GHz}$ (mJy)	Radio Morphology
J1332−3125	13 32 59.08	−31 25 17.5	1.01	unres.
J1333−3119a	13 33 00.78	−31 19 19.8	3.09	ext.
J1333−3144	13 33 01.47	−31 44 12.9	1.49	unres.
J1333−3139a	13 33 04.27	−31 39 04.0	1.50	unres.
J1333−3123	13 33 05.05	−31 23 55.5	2.20	unres.
J1333−3145a	13 33 07.07	−31 45 47.0	1.07	unres.
J1333−3147a	13 33 08.97	−31 47 33.5	0.80	unres.
J1333−3146	13 33 11.80	−31 46 50.6	0.52	unres.
J1333−3143a	13 33 15.81	−31 43 08.7	0.52	unres.
J1333−3153	13 33 17.71	−31 53 24.6	1.54	unres.
J1333−3139b	13 33 17.83	−31 39 09.2	1.56	unres.
J1333−3134	13 33 22.64	−31 34 42.0	0.62	unres.
J1333−3124	13 33 23.02	−31 24 10.0	0.52	unres.
J1333−3143b	13 33 24.58	−31 43 06.7	0.72	unres.
J1333−3125	13 33 27.32	−31 25 16.7	0.90	unres.
J1333−3156	13 33 30.11	−31 56 30.9	0.89	unres.
J1333−3141	13 33 32.00	−31 41 18.1	109.33	ext.(HT)
J1333−3138	13 33 32.11	−31 38 20.7	3.76	unres.
J1333−3130	13 33 37.29	−31 30 46.5	43.10	unres.
J1333−3147b	13 33 39.36	−31 47 06.4	0.33	unres.
J1333−3145b	13 33 40.10	−31 45 22.4	0.69	unres.
J1333−3119b	13 33 40.63	−31 19 53.5	5.94	unres.
J1333−3154	13 33 40.90	−31 54 15.3	0.45	unres.
J1333−3142	13 33 41.35	−31 42 29.0	0.50	unres.
J1333−3135	13 33 41.39	−31 35 50.0	3.14	ext.
J1333−3139c	13 33 46.24	−31 39 27.3	1.76	unres.
J1333−3128	13 33 49.64	−31 28 31.2	3.23	ext.
J1333−3139d	13 33 51.28	−31 39 36.5	1.02	unres.
J1333−3119c	13 33 52.96	−31 19 56.9	13.94	unres.
J1333−3129	13 33 57.94	−31 29 05.8	1.09	unres.
J1333−3158	13 33 58.72	−31 58 11.9	1.00	unres.
J1333−3132	13 33 59.12	−31 32 52.0	0.60	unres.
J1334−3146	13 34 03.59	−31 46 31.5	0.37	unres.
J1334−3119a	13 34 04.08	−31 19 25.5	3.78	unres.
J1334−3143	13 34 06.49	−31 43 37.4	0.97	unres.
J1334−3131a	13 34 07.80	−31 31 02.9	1.12	unres.
J1334−3128	13 34 08.32	−31 28 36.2	33.63	unres.
J1334−3136a	13 34 10.54	−31 36 57.0	3.45	ext.
J1334−3153	13 34 11.15	−31 53 36.0	0.66	unres.
J1334−3123	13 34 12.49	−31 23 54.3	6.79	unres.
J1334−3126a	13 34 13.43	−31 26 39.1	4.91	unres.
J1334−3149a	13 34 13.84	−31 49 48.6	5.51	unres.
J1334−3142	13 34 15.56	−31 42 24.7	0.40	unres.
J1334−3149b	13 34 17.71	−31 49 07.8	1.21	unres.
J1334−3131b	13 34 19.03	−31 31 08.8	1.28	unres.
J1334−3119b	13 34 22.11	−31 19 08.4	41.70	unres.
J1334−3139a	13 34 22.47	−31 39 06.8	16.77	unres.
J1334−3137	13 34 22.82	−31 37 08.3	0.74	unres.
J1334−3136b	13 34 29.22	−31 36 44.7	1.60	unres.
J1334−3141a	13 34 36.65	−31 41 01.6	2.11	unres.
J1334−3132	13 34 37.36	−31 32 47.9	26.48	ext.
J1334−3124	13 34 40.05	−31 24 56.5	5.25	unres.
J1334−3126b	13 34 40.57	−31 26 32.4	2.71	unres.
J1334−3141b	13 34 46.19	−31 41 35.7	0.95	unres.
J1334−3155	13 34 46.64	−31 55 20.2	1.38	unres.

Table 3. Continued

Name VLA−	RA_{J2000}	DEC_{J2000}	$S_{1.4GHz}$ (mJy)	Radio Morphology
J1334−3125	13 34 51.01	−31 25 25.5	3.19	unres.
J1334−3151	13 34 52.21	−31 51 10.1	3.84	unres.
J1334−3139b	13 34 54.11	−31 39 14.9	0.77	unres.
J1335−3139	13 35 02.97	−31 39 11.6	16.71	unres.
J1335−3130	13 35 08.78	−31 30 31.3	1.63	unres.
J1335−3133	13 35 12.17	−31 33 37.3	2.21	unres.
J1335−3134	13 35 18.98	−31 34 41.9	2.77	unres.

al. 1990) and finally the MGP catalogue (Metcalfe et al. 1994).

All these catalogues have a claimed positional accuracy of $\sim 0.25''$, but given the errors which could be introduced by transforming the sky image on the plate frame, we adopted a mean optical positional uncertainty of 1.5 arcsec (Unewisse et al. 1993).

The radio positional error depends on the beam size and on the source flux density (Prandoni et al. 2000). With the parameters of our observations we estimate an average position uncertainty of 2.5 arcsec both in right ascension and declination. For the faintest sources in the sample (5σ) the positional error raises to $\sim 4.2'' \times 3.5''$ along the beam axis (HPBW/(2×SNR), being SNR the signal–to–noise ratio).

In order to make sure that no identification was missed, we examined also the photometric catalogue of optical galaxies in this region in Metcalfe et al. (1994) and we overplotted all the radio sources in our sample on the optical red Digitized Sky Survey DSS–2 images and carried out a careful visual inspection.

Given the uncertainty in the radio and optical positions, in order to estimate the reliability of the optical identifications, we adopted the parameter $\mathcal{R}$, defined as:

$$\mathcal{R}^2 = \frac{\Delta^2_{r-o}}{\sigma_o^2 + \sigma_r^2}$$

where Δ_{r-o} is the positional offset between radio and optical coordinates and σ_o= 1.5 arcsec and σ_r= 2.5 arcsec are the optical and radio position errors respectively.

We considered reliable identifications all matches with $\mathcal{R} \leq 3$. Given the extent of the radio emission we found $\mathcal{R} > 3$ for a number of sources, but we considered them reliable identifications since the optical counterpart falls within the radio isophotes (further details are given in Appendix).

The reliability (*rel*) and completeness (*comp*) of our sample of identified radio sources was tested following the method suggested by de Ruiter et al. (1977). We note that the reliability represents the fraction of true, i.e. non spurious, optical identifications in the sample, while the completeness provides the fraction of true identifications found with respect to the total number of IDs in the sample. For $\mathcal{R} = 3$ we found *rel* = 96.3% and *comp* = 97.8%; while for $\mathcal{R} = 2$ we have *rel* = 99% and *comp* = 68.3%. We note that completeness drops considerably going from $\mathcal{R} = 3$ to $\mathcal{R} = 2$. For this reason, and in the light of the puropse of the present paper (see Sections 6.1, 6.3, 7.1 and 7.2), we consider $\mathcal{R} = 3$ as the most appropriate choice.

The list of the radio-optical identification is reported in Table 4, where we give:
− column 1 : radio and optical name, where # stands for optical counterparts from Bardelli et al. (1994, 1998b) and MGP94 from Metcalfe et al. (1994);
− columns 2 and 3: J2000 radio and optical coordinates;
− column 4: radio flux density at 1.4 GHz and b_J magnitude;
− column 5: radio morphology and optical type, where E = elliptical, S = spiral, IS = interacting system, qso = quasar candidate;
− column 6: radio power at 1.4 GHz and radial velocity;
− column 7: $\mathcal{R}$ parameter and (B–R) colours for the optical counterparts in the Shapley Concentration taken from Metcalfe et al. (1994).

The morphological classification of the optical objects given in Table 4 was done by inspection of the DSS–2 images. The redshift information is taken from Bardelli et al. (1994, 1998b) and Metcalfe et al. (1994).

We found 68 identifications, corresponding to ∼40% of our radio source sample. Among these, 33 (48% of the identified sources) are located at the redshift of the Shapley Concentration (velocity range $\sim 11000 - 17500$ km s^{-1}, Bardelli et al. 1998b).

6. The radio emission in A3558–C

6.1. General comments on the radio galaxies

The sample of 33 optically identified radio sources in A3558–C includes 18 early–type galaxies and 14 spirals. The optical morphology of J1333−3124 is unavailable (see Table 4).

In Figure 2 and 3 we show the 1.4 GHz radio contours respectively of the late– and early–type radio galaxies, overlaid on the DSS–2 optical frame. We note that the radio galaxy J1332–3146a is shown separately in Fig. 4; the radio halo at the centre of A3562, including the radio galaxy J1333–3141 is given in Fig. 5; and finally J1333–3124 is included among the early–type galaxies (Fig. 3).

Table 4. Optical Identifications

Radio Name VLA− Opt. Name	RA_{J2000} RA_{J2000}	DEC_{J2000} DEC_{J2000}	$S_{1.4GHz}$ (mJy) b_J	Radio type Opt.type	$\log P_{1.4GHz}$ h^{-2} (W Hz^{-1}) v (km s^{-1})	$\mathcal{R}$ B–R
J1329−3126	13 29 00.02	−31 26 26.0	81.92	ext.	–	2.88
	13 29 00.22	−31 26 34.0	18.96	qso	–	–
J1329−3119a	13 29 49.32	−31 19 37.3	6.02	unres.	–	1.58
	13 29 49.02	−31 19 39.9	15.09	–	–	–
J1329−3122a	13 29 50.76	−31 22 55.6	22.43	unres.	24.00	1.17 ◇
#10178	13 29 50.8	−31 22 59	19.08	E	58755	–
J1329−3057	13 29 51.22	−30 57 47.2	65.38	unres.	–	1.34
	13 29 51.44	−30 57 49.8	22.15	–	–	–
J1329−3119b	13 29 55.02	−31 19 57.7	4.53	unres.	22.07	0.10
#10174	13 29 55.00	−31 19 57.6	15.15	S	14799	2.05
J1330−3124a	13 30 05.10	−31 24 36.3	6.89	unres.	22.20	0.41
#10318	13 30 05.05	−31 24 37.2	16.05	S	13770	1.86
J1330−3113	13 30 05.59	−31 13 44.8	1.79	unres.	21.76	3.70
#10313	13 30 05.09	−31 13 53.5	17.44	S	15942	1.53
J1330−3144b	13 30 08.56	−31 44 02.8	3.26	unres.	23.06	2.50
#10332	13 30 09.05	−31 43 59.0	19.34	–	52606	–
J1330−3124b	13 30 10.06	−31 24 05.6	5.81	unres.	–	1.58
	13 30 10.16	−31 24 01.2	22.13	–	–	–
J1330−3122	13 30 19.06	−31 22 58.2	439.08	unres.	–	0.31
	13 30 19.1	−31 22 59	18.46	qso	–	–
J1330−3153	13 30 33.03	−31 53 29.1	1.14	unres.	–	1.13
	13 30 32.85	−31 53 31.5	18.03	–	–	–
J1330−3134	13 30 41.21	−31 34 17.4	3.86	ext.	22.06	0.41
#10725	13 30 41.29	−31 34 16.9	16.40	S	15524	1.72
J1330−3143b	13 30 47.95	−31 43 40.2	7.77	ext.	22.25	2.30 ◇
#10869	13 30 47.95	−31 43 33.5	15.58	S	13894	–
J1330−3146	13 30 51.97	−31 46 00.0	1.98	unres.	21.66	2.74
#10871	13 30 52.13	−31 46 07.8	17.79	E	13832	1.86
J1330−3209	13 30 52.00	−32 09 02.3	0.73	unres.	21.17	2.09
#10888	13 30 52.08	−32 08 56.3	16.55	S	12932	1.78
J1330−3127	13 30 52.33	−31 27 01.1	1.04	unres.	21.44	4.70 ◇
#10986	13 30 52.59	−31 27 14.1	17.76	E	14618	1.94
J1331−3144	13 31 00.60	−31 44 51.4	2.55	unres.	21.67	0.75
#11000	13 31 00.65	−31 44 53.6	16.98	S	12141	1.68
J1331−3140	13 31 01.87	−31 40 35.3	0.60	unres.	21.10	0.55
#10996	13 31 01.91	−31 40 36.8	18.22	E	13178	1.67
J1331−3139	13 31 12.00	−31 39 27.1	9.48	unres.	–	3.81 ◇
	13 31 11.6	−31 39 37	17.97	qso	–	–

Table 4. Optical Identifications. Continued

Radio Name VLA− Opt. Name	RA_{J2000} RA_{J2000}	DEC_{J2000} DEC_{J2000}	$S_{1.4GHz}$ (mJy) b_J	Radio type Opt.type	$\log P_{1.4GHz}$ h^{-2} (W Hz^{-1}) v (km s^{-1})	$\mathcal{R}$ B–R
J1331−3155a	13 31 14.14	−31 55 49.2	0.78	unres.	–	1.34
	13 31 14.38	−31 55 46.8	20.47	–	–	–
J1331−3135	13 31 16.85	−31 35 34.2	0.93	unres.	21.39	2.47
MGP94 3226	13 31 17.32	−31 35 38.1	17.13	E	14578	1.53
J1331−3128	13 31 16.91	−31 28 20.1	22.28	unres.	–	2.98
	13 31 17.3	−31 28 13	17.72	qso	–	–
J1331−3113	13 31 18.79	−31 13 56.2	2.38	unres.	21.83	4.63
#11243	13 31 19.38	−31 13 45.0	16.35	S	15710	1.97
J1331−3143	13 31 19.88	−31 43 50.2	14.53	ext.	–	2.71 ⋄
	13 31 19.84	−31 43 42.3	19.36	–	–	–
J1331−3149a	13 31 27.54	−31 49 14.7	1.32	unres.	21.44	0.62
MGP94 3303	13 31 27.4	−31 49 14.5	15.64	E	12928	2.05
J1331−3133a	13 31 37.66	−31 33 08.4	3.69	unres.	21.95	0.45
#11515	13 31 37.57	−31 33 07.7	15.71	E	14205	–
J1331−3206	13 31 42.95	−32 06 38.2	129.85	unres.	–	2.54
	13 31 42.8	−32 06 31	17.20	qso	–	–
J1331−3148	13 31 50.22	−31 48 47.4	1.32	unres.	21.46	3.09
#11639	13 31 50.77	−31 48 41.7	16.45	E	13343	–
J1331−3142	13 31 50.89	−31 42 49.7	2.13	unres.	–	0.82
	13 31 51.01	−31 42 47.9	22.80	–	–	–
J1331−3155b	13 31 53.27	−31 55 33.4	2.06	unres.	–	0.99 ⋄
#11647	13 31 53.22	−31 55 36.2	19.08	E	–	–
J1331−3154c	13 31 54.83	−31 54 01.2	1.19	unres.	21.40	1.13
#11644	13 31 54.77	−31 54 04.4	17.52	E	13028	1.84
J1331−3149b	13 31 59.47	−31 49 19.8	1.82	ext.	21.58	1.54
#11751	13 31 59.72	−31 49 23.1	17.46	S	12963	–
J1332−3136a	13 32 00.29	−31 36 26.4	0.40	unres.	–	1.65
	13 32 00.65	−31 36 24.8	19.19	–	–	–
J1332−3146a	13 32 02.78	−31 46 50.0	15.11	ext.	22.52	0.99
#11744	13 32 03.02	−31 46 49.9	14.96	E	13107	2.07
J1332−3152a	13 32 05.13	−31 52 30.4	0.49	unres.	21.04	1.99
#11753	13 32 05.58	−31 52 30.0	16.41	S	13634	1.67
J1332−3141a	13 32 05.34	−31 41 23.4	11.32	unres.	–	0.72 ⋄
	13 32 05.47	−31 41 24.7	19.85	–	–	–
J1332−3131a	13 32 15.98	−31 31 25.7	0.83	unres.	–	2.40
#11872	13 32 15.89	−31 31 32.6	18.08	S	–	–
J1332−3152b	13 32 17.52	−31 52 49.6	15.78	unres.	–	0.75
	13 32 17.68	−31 52 50.4	22.46	–	–	–

Table 4. Optical Identifications. Continued

Radio Name VLA− Opt. Name	RA_{J2000} RA_{J2000}	DEC_{J2000} DEC_{J2000}	$S_{1.4GHz}$ (mJy) b_J	Radio type Opt.type	$\log P_{1.4GHz}$ h^{-2} (W Hz^{-1}) v (km s^{-1})	$\mathcal{R}$ B–R
J1332−3131b	13 32 35.38	−31 31 41.8	1.79	unres.	21.71	1.61
#12072	13 32 35.24	−31 31 46.2	17.28	E	15193	1.36
J1332−3135	13 32 37.56	−31 35 55.5	0.76	unres.	–	1.85
	13 32 37.98	−31 35 54.9	15.80	–	–	–
J1332−3155	13 32 43.25	−31 55 11.0	0.58	unres.	21.18	2.19
#12200	13 32 42.85	−31 55 14.8	16.96	E	14483	1.73
J1332−3146b	13 32 43.92	−31 46 53.2	1.41	unres.	21.46	2.92
#12195	13 32 43.87	−31 47 01.7	17.33	E	12836	1.58
J1332−3142a	13 32 44.59	−31 42 44.8	0.34	unres.	–	0.75
	13 32 44.75	−31 42 57.0	19.13	–	–	–
J1332−3136b	13 32 46.59	−31 36 58.5	1.92	unres.	21.56	1.82
#12190	13 32 46.44	−31 37 03.4	16.88	E	12317	1.34
J1332−3156	13 32 50.23	−31 56 11.5	0.76	unres.	–	0.89
	13 32 50.33	−31 56 09.2	20.92	–	–	–
J1332−3134	13 32 56.48	−31 34 52.5	0.72	unres.	–	0.82
	13 32 56.34	−31 34 51.0	19.63	–	–	–
J1333−3144	13 33 01.47	−31 44 12.9	1.49	unres.	–	2.50
#12286	13 33 01.24	−31 44 19.6	18.50	S	–	–
J1333−3139a	13 33 04.27	−31 39 04.0	1.50	unres.	21.57	0.82
#12372	13 33 04.08	−31 39 04.6	18.32	S	14120	1.85
J1333−3123	13 33 05.05	−31 23 55.5	2.20	unres.	–	0.99
	13 33 05.12	−31 23 58.2	20.24	–	–	–
J1333−3124	13 33 23.02	−31 24 10.0	0.52	unres.	21.04	5.04
#12572	13 33 23.46	−31 24 23.6	17.32	–	13103	1.94
J1333−3141	13 33 32.00	−31 41 18.1	109.33	HT	23.43	6.58
MGP94 4108	13 33 31.5	−31 41 00	17.25	E	14438	2.09
J1333−3130	13 33 37.29	−31 30 46.5	43.10	unres.	–	0.45
	13 33 37.2	−31 30 46	22.42	–	–	–
J1333−3119b	13 33 40.63	−31 19 53.5	5.94	unres.	–	2.23
#12661	13 33 40.60	−31 19 60.0	16.64	IS	–	–
J1333−3135	13 33 41.39	−31 35 50.0	3.14	ext.	–	0.31
	13 33 41.36	−31 35 49.2	21.96	–	–	–
J1333−3128	13 33 49.64	−31 28 31.2	3.23	ext.	21.68	4.25
#12779	13 33 50.37	−31 28 39.2	16.59	E	10994	1.50
J1333−3129	13 33 57.94	−31 29 05.8	1.09	unres.	–	6.45
	13 33 57.17	−31 29 21.8	17.45	E	–	–
J1333−3158	13 33 58.72	−31 58 11.9	1.00	unres.	21.43	1.78
#12912	13 33 58.68	−31 58 17.0	17.75	S	14689	1.75

Table 4. Optical Identifications. Continued

Radio Name VLA− Opt. Name	RA_{J2000} RA_{J2000}	DEC_{J2000} DEC_{J2000}	$S_{1.4GHz}$ (mJy) b_J	Radio type Opt.type	$logP_{1.4GHz}$ h^{-2} (W Hz^{-1}) v (km s^{-1})	$\mathcal{R}$ B–R
J1334−3143	13 34 06.49	−31 43 37.4	0.97	unres.	–	4.80
MGP94 4345	13 34 06.5	−31 43 39	18.48	–	–	–
J1334−3153	13 34 11.15	−31 53 36.0	0.66	unres.	–	0.62
	13 34 11.25	−31 53 34.8	18.39	E	–	–
J1334−3149b	13 34 17.71	−31 49 07.8	1.21	unres.	–	1.96
#13013	13 34 18.16	−31 49 08.0	17.25	S	–	–
J1334−3119b	13 34 22.11	−31 19 08.4	41.70	unres.	–	3.40
	13 34 22.3	−31 19 18	20.63	–	–	–
J1334−3137	13 34 22.82	−31 37 08.3	0.74	unres.	–	0.99
	13 34 23.00	−31 37 10.0	21.12	–	–	–
J1334−3141a	13 34 36.65	−31 41 01.6	2.11	unres.	21.52	3.91
#13198	13 34 35.87	−31 41 07.0	16.48	S	11357	–
J1334−3132	13 34 37.36	−31 32 47.9	26.48	ext.	22.86	11.46 ⋄
#13281	13 34 39.9	−31 32 55	17.30	E	16490	1.80
J1334−3126b	13 34 40.57	−31 26 32.4	2.71	unres.	21.82	3.88
#13277	13 34 40.76	−31 26 43.4	17.09	E	14156	1.68
J1335−3139	13 35 02.97	−31 39 11.6	16.71	unres.	22.66	3.09
#13503	13 35 03.14	−31 39 20.3	15.73	E	15077	2.07
J1335−3133	13 35 12.17	−31 33 37.3	2.21	unres.	21.69	3.33
#13629	13 35 12.59	−31 33 45.5	16.36	S	13673	1.50
J1335−3134	13 35 18.98	−31 34 41.9	2.77	unres.	23.08	5.63
#13630	13 35 18.86	−31 34 58.2	18.17	–	58050	–

Notes to Table 4: ⋄ see comments in Appendix.

In Figure 6 we show the location of the A3558–C early– and late–type radio galaxies listed in Table 4, overlaid on the 1.4 GHz radio contours of the same region. No difference in the bidimensional distribution of these two classes is obvious from the figure.
In search for possible segregation effects in the location of the 33 radio galaxies detected in this survey, we examined the velocity distribution of the optical counterparts, and compared it to that of all optical galaxies belonging to the A3558–C region covered in our survey. The optical catalogue was extracted from the sample in Bardelli et al. (1994, 1998b). The radio galaxies appear to be uniformly distributed over the Shapley supercluster velocity range, with a peak of nine objects at ~ 13000 km s^{-1} (Fig. 7). Six of them belong to the SC 1329-313 group and in particular to the T520 subclump (Bardelli et al. 1998a).

6.2. The diffuse radio galaxy J1332-3146a

A remarkable feature of the radio emission in A3558–C is the very low brightness extended tail associated with the radio galaxy J1332−3146a. This source is identified with the cluster galaxy #11744 ($b_J = 14.96$ and velocity $v = 13107$ km s^{-1}, see Table 4), the brightest galaxy in the group SC 1329–313. The projected angular size of the radio emission is $\sim 6' \times 4'$, corresponding to $\sim 240 \times 160$ kpc. The radio power is $logP_{1.4GHz}$ (W Hz^{-1}) = 22.52 and its surface brightness is ~ 0.16 mJy b^{-1}.
We note that the X–ray emission in this region is elongated in the direction of A3562, and compressed towards SC 1327–312, and J1332–3146a is located at the border of the X–ray emission of the SC 1329 group, as clear from Figure 4.

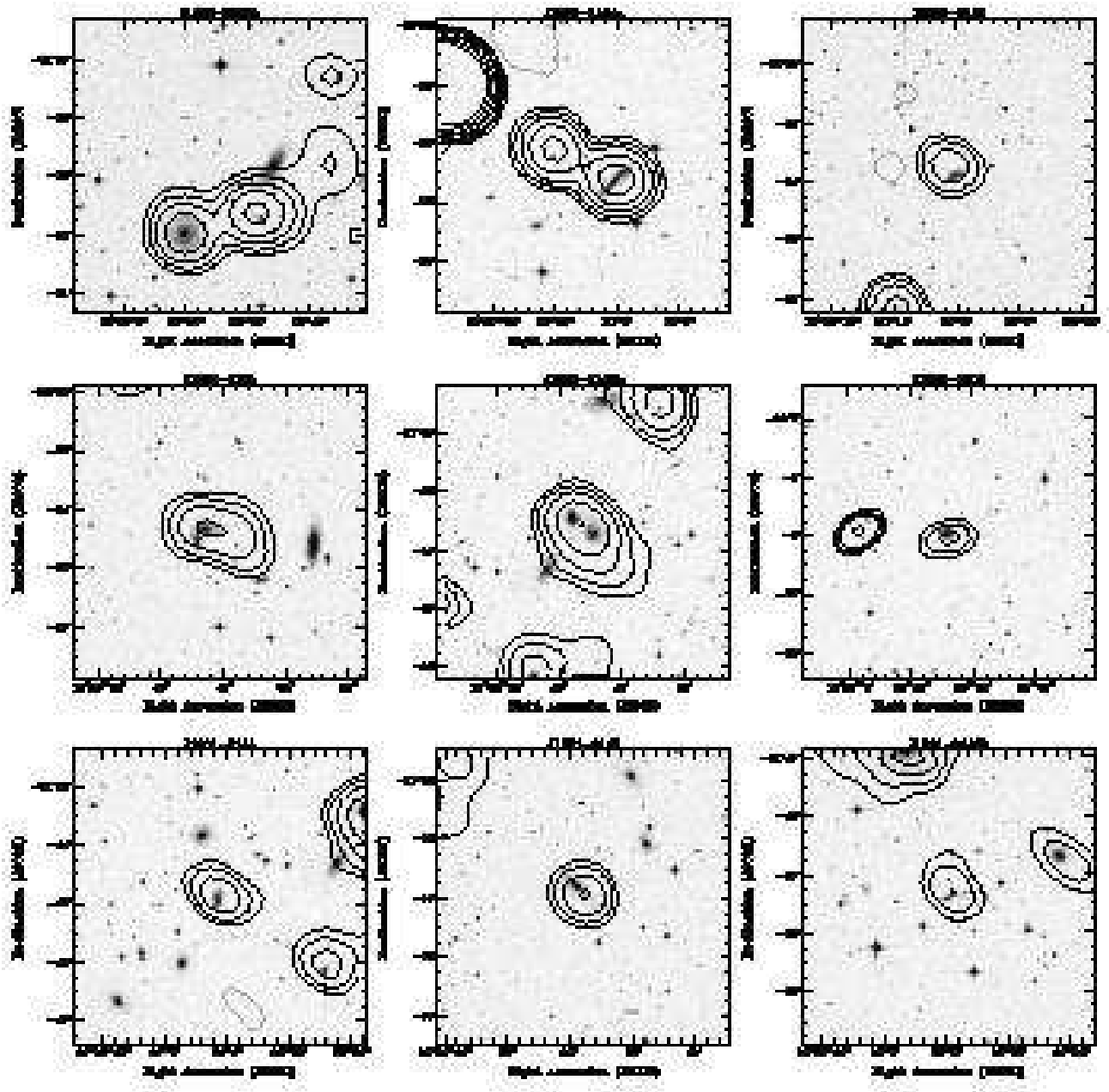

Fig. 2. 1.4 GHz radio contours of the 14 late–type radio galaxies in A3558–C overlaid on the DSS–2 optical frame. Radio contours are as follows. For J1330−3209: –0.25, 0.25, 0.30, 0.35, 0.50, 1.00, 2.00 mJy b^{-1}; for J1332−3152a: –0.25, 0.25, 0.30, 0.50, 1.00, 2.00 mJy b^{-1}; for J1335−3133: –0.50, 0.50, 0.75, 1.00, 1.50, 2.00 mJy b^{-1}. for all remaining radio galaxies: –0.25, 0.25 0.50, 1.00, 2.00 mJy b^{-1}; The restoring beam is $41.98'' \times 35.13''$, p.a. 55.7°.

The presence of extended emission associated with J1332−3146a was suggested by inspection of 843 MHz Molonglo Observatory Synthes Telescope (MOST) observations and of the NVSS 1.4 GHz image, where the source has a projected angular size of $\sim\ 4' \times\ 2'$ (V2000). The overall morphology in our image (Figure 4) is in very good agreement with the NVSS image.

J1332−3146a was detected as point–like with the ATCA both at 22 cm and 13 cm, at the resolution of a few arcseconds, and the derived spectral index is α_{13}^{22} = 0.81 (V2000). We note that the source was labelled J1332−3146 in V2000. The compact morphology and steep spectrum at high resolution seem to rule out any connection between the low brightness extended emission and an active nucleus. In other words, there is no indication that the extended emission imaged with the observations presented here is a tail of a head–tail or wide–angle tail radio source.

In Figure 5 the radio contours of the A3558–C region between the radio halo at the centre of A3562 and

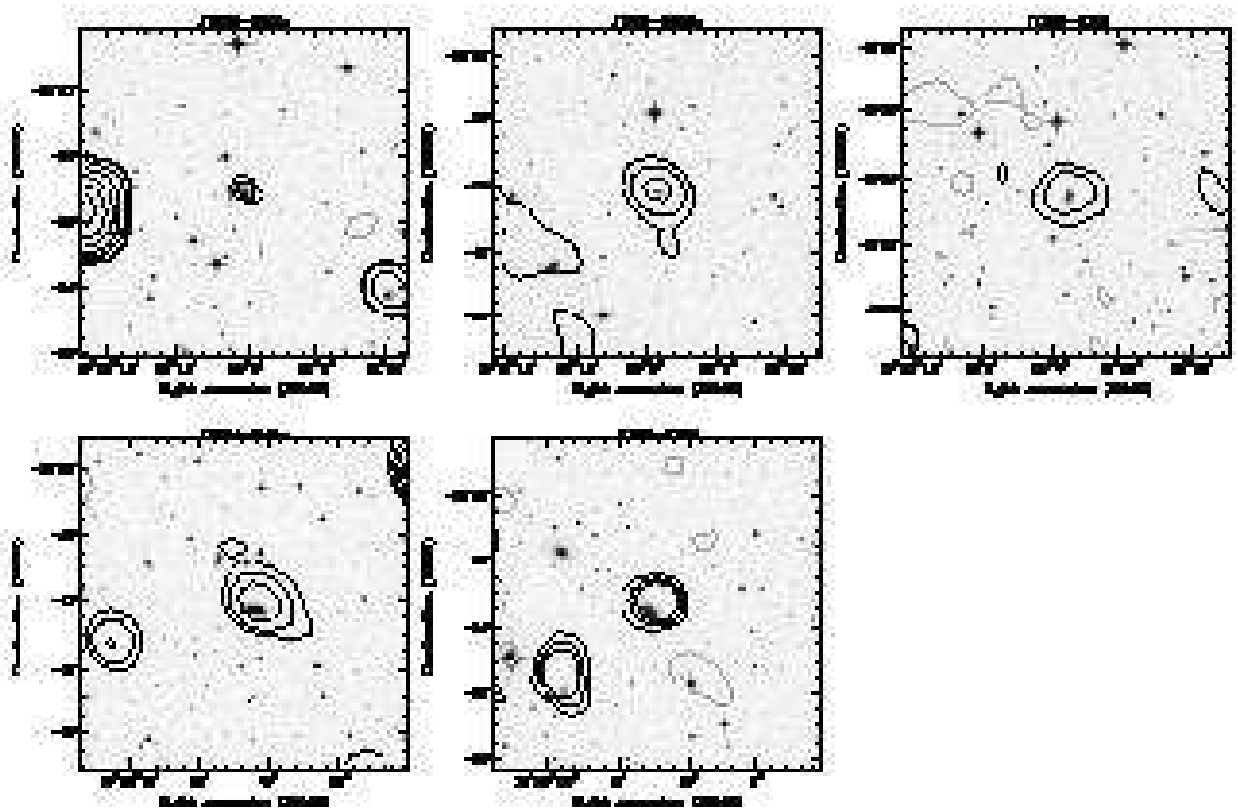

Fig. 2. Continued.

J1332–3146a are superposed to the DSS–2 optical frame. Inspection of the radio emission in this region suggests some important considerations. In particular, *(a)* the extension of J1332–3146a points towards the radio halo at the centre of A3562; *(b)* the radio halo is characterised by a filament pointing South–West, towards J1332–3146a; *(c)* positive residuals of radio emission are clearly visible in the region between the radio halo and J1332–3146a. Excluding the strongest point sources (with flux density S$> 5\sigma$), these residuals account for several mJy.

It is possible that the extended emission in J1332–3146a is *(i)* part of a very low brightness cluster scale bridge of emission, extending from the centre of A3562 to the smaller group SC 1329–313, undetectable with the radio instrumentation presently available; *ii)* the result of reacceleration processes and can therefore be interpreted as *revived* radio emission. We remind here that J1332−3146a lies in a region where a merger shock is expected, on the basis of numerical simulations and of the properties of the X–ray emission.

6.3. The population of faint radio galaxies in A3558–C. Enhanced radio activity due to a cluster merger?

An indicator of starburst activity is the presence of radio emission at power levels of the order $P_{1.4\ GHz} \lesssim 10^{23} h^{-2}$ W Hz^{-1} (see Condon et al. 2002 for a recent discussion). The majority of the A3558–C radio galaxies in our list has radio power below this threshold. In particular, 12 out of 18 radio emitting ellipticals have log$P_{1.4\ GHz}$ (W Hz^{-1}) $<$ 21.78, the lower limit of the radio luminosity function for AGNs derived by LO96 (scaled to the cosmology adopted in our paper) discussed in Section 7.1. Among the spiral galaxies with associated radio emission, they all have log$P_{1.4\ GHz}$ (W Hz^{-1}) ≤ 22.25. Including the radio galaxy J1333–3124, whose optical counterpart has no morphological classification, the total number of candidate starburst radio galaxies in our sample is therefore 26.

A detailed optical study of the spectral properties of the galaxies in A3558−C shows that the region between A3562 and the SC groups is populated by a very large fraction of blue galaxies (Bardelli et al. 1998b). To quantify this effect we considered the (B–R) colours of the photometric sample of optical galaxies in this region of Metcalfe et al. (1994): from a b_J vs (B–R) plot we found that the red sequence is at (B–R) $\sim$ 2 and we set (B–R) < 1.7 as the limit to define a blue object. We cross–correlated our sample of faint radio galaxies with the sample of Metcalfe et al. (1994) and found that 4 spirals and 7 ellipticals are blue. Beyond that, we note that the (B–R) values for all the radio galaxies in A3558–C are lower than the average value for A3558–C [$<$(B–R)$>$ $\sim$ 2], with few very extreme cases (see Table 4). In conclusion, for half

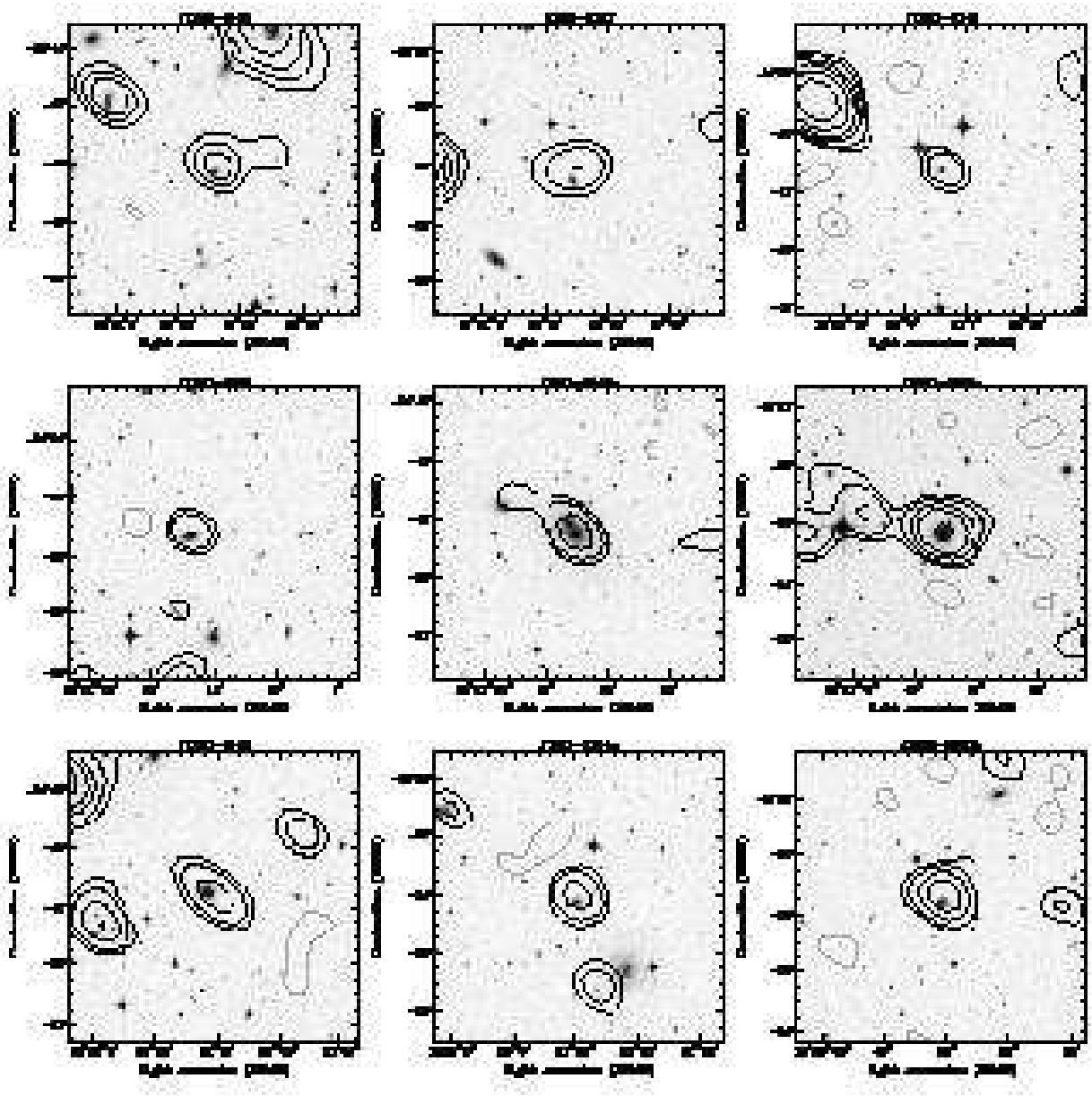

Fig. 3. 1.4 GHz radio contours of the early–type radio galaxies in A3558–C overlaid on the DSS–2 optical frame. Radio contours are: –0.175, 0.175, 0.3, 0.6, 1, 2, 4, 8, 16 etc. mJy b^{-1}. For J1330−3146 and J1334−3126b the lowest contour is –0.3, 0.3 mJy b^{-1}. The restoring beam is $41.98'' \times 35.13''$, p.a. 55.7°.

of the faint radio sources in the region under study, indication of starburst radio emission is supported by photometric information. Assuming that there is no contribution from an active nucleus, the star formation rates (SFR) deduced on the basis of the radio emission are in the range SFR$\sim$ $1.2 \div 7.1$ M$_\odot$ yr^{-1}. This estimate was done using the empirical relation between SFR and radio luminosity in Yun et al. (2001), after scaling our radio luminosity to the cosmology used in their paper.

We compared our results on A3558–C with those obtained by MO03 for A2255, whose radio emission was interpreted in terms of increased radio AGN activity and star formation as consequence of the cluster merger.
For a proper comparison we needed to apply some transformations and corrections to our data. In particular:

(i) first of all, for our COSMOS b_J magnitudes, we considered a correction according to Lumsden et al. (1997) for a "saturation" effect which occurs for bright objects due to the lack of dynamic range within the measuring machine; then we assumed $b_J \simeq m_B$ (as found by Bardelli et al. 2000) and applied a correction for the galactic absorption of $A_B = 0.24$ (Schlegel et al. 1998). We converted our mag-

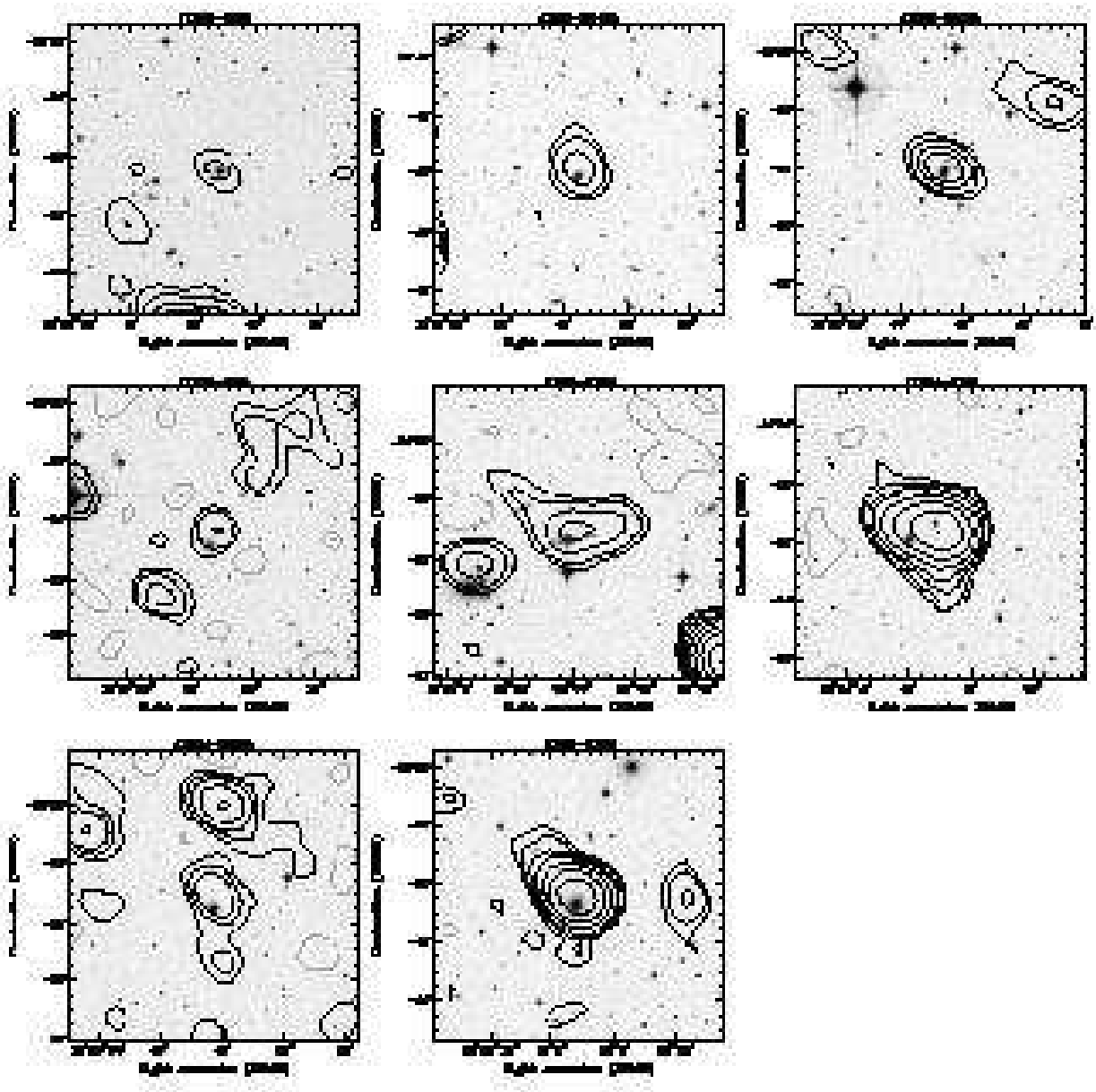

Fig. 3. Continued.

nitudes to the m_{Rc} magnitudes using the (B–R_c) colours in Fukugita et al. (1995): we adopted (B–R_c) = 1.48 for early-type galaxies (average value between E and S0) and (B–R_c) = 1.00 for late-type galaxies (average value between spirals and Irr). Finally we computed the M_R magnitudes for our sample adopting the MO03 cosmology.

(ii) We rescaled the radio powers of our A3558–C radio galaxies to the MO03 cosmology, and selected only those sources with $\log P_{1.4\ GHz}$ (W Hz^{-1}) $\geq$ 21.84.

(iii) We extracted a normalization sample from the COSMOS catalogue containing all galaxies within the MO03 limit $M_R \leq -20$ in the region of A3558–C covered by our observations. We applied the same magnitude corrections described in point (i). In this case we adopted an average (B–R_c) = 1.36 with the assumption of a morphological mix of 73% ellipticals and 27% spirals in this region. From the number counts of this sample we subtracted the contribution of field galaxies determined from the ESP survey (Vettolani et al. 1997) which was obtained from the COSMOS catalogue. Also for these objects we considered the same magnitude corrections as in point (i) with $A_B = 0$ (the ESP survey is at the galactic pole) and (B–R_c) = 1.15 which corresponds to a morphological mix for the field of 30% early–type and 70% late–type galaxies.

Following MO03 we divided our optical sample in three magnitude bins, i.e. "faint" ($-21 < M_R \leq$ -20), "interme-

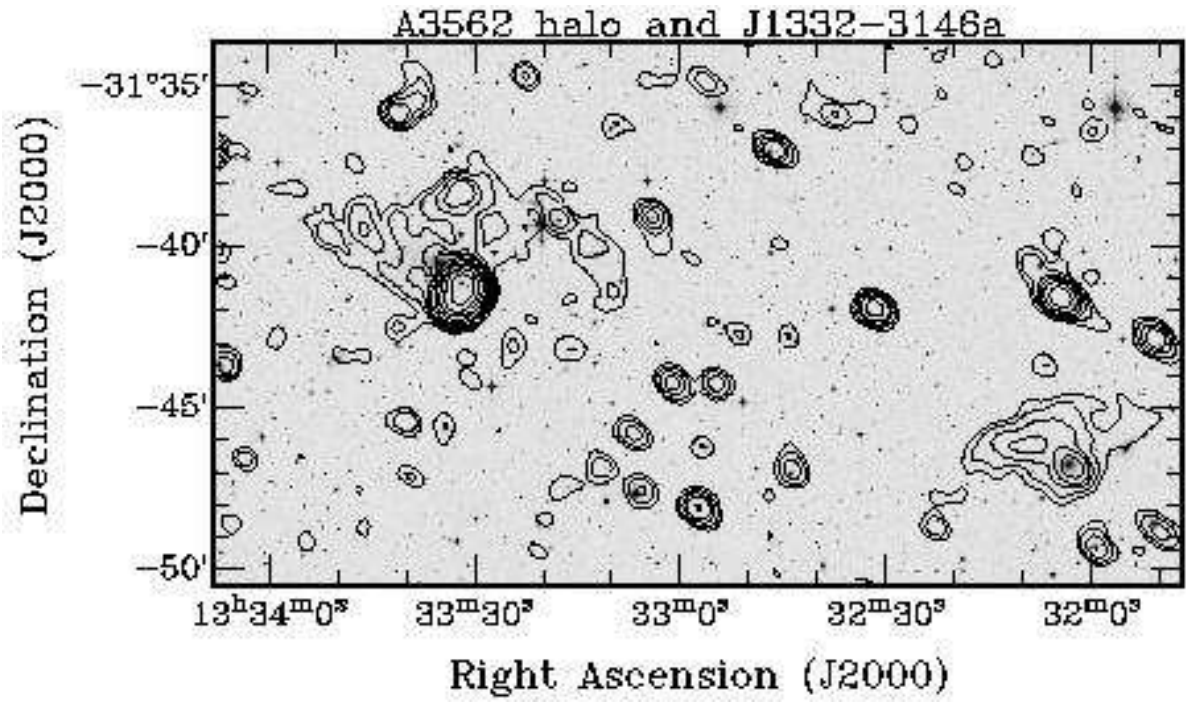

Fig. 5. 1.4 GHz radio contours of the A3558–C region between the A3562 central radio halo and the extended radio galaxy J1332–3146a, overlaid on the optical DSS–2 red frame. Contours are –0.15, 0.15, 0.3, 0.6, 1, 2, 4, 8, 16, 32, 64, 128, 250 mJy b^{-1}. The restoring beam in the image is $41.98'' \times 35.13''$, in p.a. 55.7°.

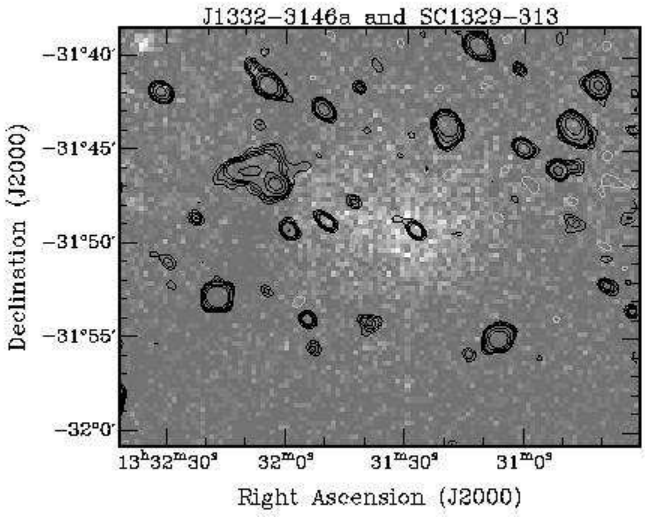

Fig. 4. 1.4 GHz VLA radio emission from the group SC 1329–313 (grey scale) superposed to the ROSAT X–ray emission. The extended radio galaxy J1332–3146a is located just outside the X–ray peak, in the North–East direction. The FWHM of the restoring beam of the radio image is $41.98'' \times 35.13''$, in p.a. 55.7°. The radio contours are –0.2, 0.2, 0.3, 0.4, 0.5, 1, 2 mJy b^{-1}.

diate" ($-22 < M_R \leq -21$) and "bright" ($M_R \leq -22$), and computed the fraction $\frac{N_{rg}}{N_{gal}}$ in each luminosity bin, including all optical morphological types. As in their paper, N_{gal} and N_{rg} are respectively the total number of optical galaxies and the total number of radio galaxies in each bin. The results of our analysis are given in Table 5 where we also report the numbers for A2255 and the mean and the dispersion for all the other clusters considered by MO03 in the 2Mpc case. We note that the fractions and errors associated with the MO03 clusters were computed by us using the numbers given in their paper.

Not surprisingly, the ratio $\frac{N_{rg}}{N_{gal}}$ increases going from the faint to the bright optical bin both in A3558–C and in A2255. If we take into account the associated errors, there is only marginal evidence of enhanced fraction of radio emitting galaxies in A3558–C and in A2255 compared to the other clusters considered in MO03.

7. Statistical analysis of A3558–C: radio/optical properties

The radio luminosity function (RLF) is a powerful statistical tool to investigate the radio properties of a galaxy population. In order to understand if the ongoing major merger in A3558–C has significant effect on the radio emission of the cluster galaxy population, it is important to compare the radio luminosity function (RLF) for galaxies in this merging environment with the mean RLF for galaxies in normal clusters and in the field.
With this aim we computed the RLF for the radio galaxies in the A3558–C and compared our results with those obtained by LO96 and by Gavazzi & Boselli (1999, hereinafter GB99) respectively for early– and late–type galaxies.

For the comparison we adopted the cosmology used by these authors and scaled the radio powers of our sample.

Table 5. Radio–optical galaxy counts

Mag Interval	N_{rg}	N_{gal} (A3558–C)	%	% (A2255)	% Other clusters
$-21 < M_R \leq -20$	3	88.4	3.4%±2.0	7.2%±2.7	1.6%±1.4
$-22 < M_R \leq -21$	9	37.8	23.8%±7.9	15.3%±4.8	20.3%±12.8
$M_R \leq -22$	6	13.7	43.8%±17.9	56.5%±21.3	23.3%±23.1

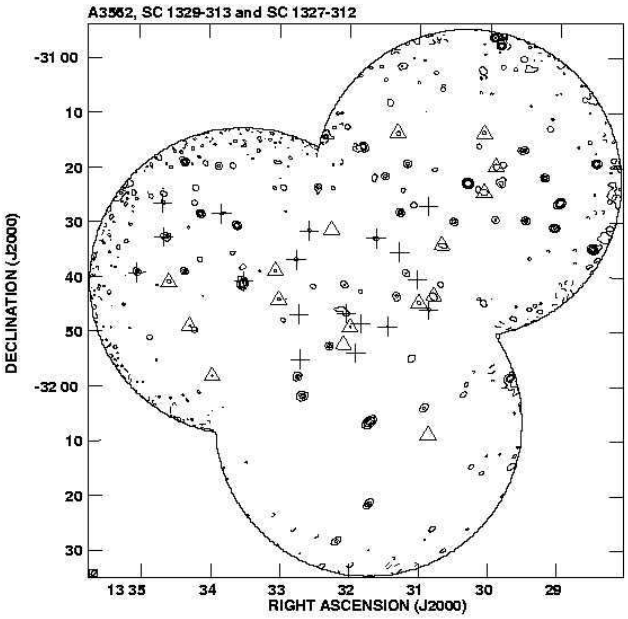

Fig. 6. Location of the Shapley Concentration optical counterparts overlaid on the 1.4 GHz radio contours of the A3562 and SC groups region. Triangles represent late–type galaxies and crosses stand for early–type galaxies. The radio contours are –0.85, 0.85, 6.80, 13.60 and 54.40 mJy b^{-1}. The galaxy without optical classification was included among the early–type galaxies.

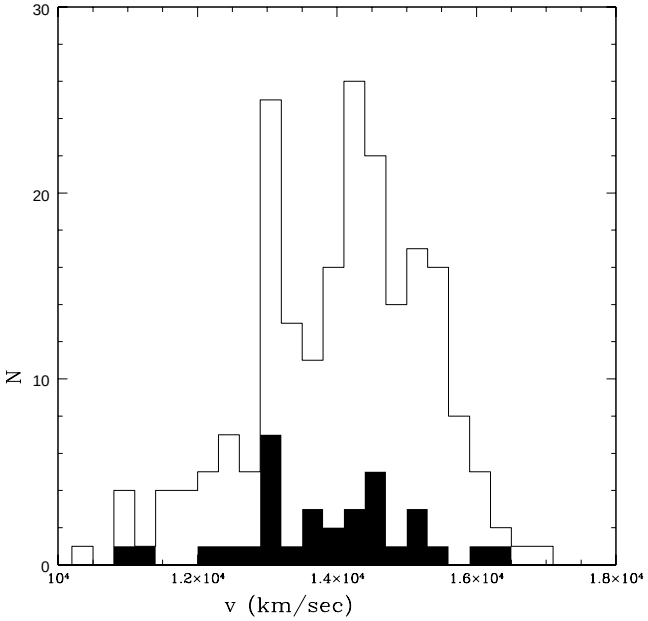

Fig. 7. Histogram of the velocity distribution of the radio galaxies in the A3562 and SC groups region given in Table 4 (black bins), compared to the velocity distribution of all galaxies in the Shapley Concentration. The width of each velocity bin is 300 km s^{-1}.

We corrected our b_J magnitudes as described in point (i) of Section 6.3.

7.1. The radio luminosity function of AGNs

We computed the number of radio galaxies expected in the A3558–C region on the basis of the "universal" RLF derived by LO96 and compared it to the number of objects actually detected in our survey.

The analysis carried out by LO96 includes radio galaxies with $\log P_{1.4\ GHz}$(W Hz^{-1}) ≥ 22.03 and optical counterparts brighter than $M_R = -20.5$. This magnitude limit corresponds to $m_R = 16.05$ at the distance of the Shapley supercluster.

We estimated that the total number of early–type galaxies in the A3558–C region located at the distance of the Shapley Concentration is 65 (see V2000 for further details). On the basis of LO96, the fraction of early−type galaxies with $M_R \leq -20.5$ expected to be radio loud at a power level $\log P_{1.4\ GHz}$(W Hz^{-1}) ≥ 22.03 is 6 ($\sim 9.2\%$), in good agreement with the seven radio galaxies in our sample matching the LO96 constraints.

Conversely, V2000 found that the RLF for early–type galaxies of the whole A3558 complex, including the cluster A3558 and the westernmost A3556, is significantly lower than the "universal" RLF by LO96. These results suggest that the effect of cluster merger on the AGN–type radio emission may be a very complex phenomenon, possibly depending on the stage of the merger. This issue will be further discussed in Section 8.

7.2. The radio luminosity function of late–type galaxies

The role of environment on the radio emission of spiral galaxies has been investigated in a number of papers. Jaffe & Perola (1976) found that radio emitting spirals in the Coma cluster have a radio excess compared to field galaxies. Gavazzi & Jaffe (1986) confirmed these results by com-

paring the RLF of late–type galaxies within and outside rich clusters. GB99 computed the RLF of spiral galaxies, in terms of radio–optical flux density ratio, in nearby different environments (rich and poor clusters, and the field), and found that late–type galaxies in rich clusters develop radio sources more frequently than galaxies in poor clusters and in the field. They also found a correlation between the radio excess and the velocity deviations with respect to the cluster average velocity. GB99 suggested that these results are coherent with a ram pressure scenario: galaxies in fast motion through the intracluster medium experience enough dynamical pressure to compress their magnetic field on the up-stream side, form a tail-like radio structure on the down-stream side and produce a net enhancement of the radio continuum activity.

We addressed the question whether the late–type galaxy population in the merging environment of the A3558–C region behaves like those in rich clusters, or if it shows even more enhanced radio excess. To this aim we compared the RLF of late–type galaxies in this region with the results obtained by GB99. We extracted a subsample of 209 objects from the GB99 sample, with Zwicky magnitude $m_z < 15.7$ and flux density $S_{1.4GHz} \geq 2.25$ mJy, corresponding to the 5σ level of the NVSS survey (radio data in GB99 are taken mostly from this survey). This flux density limit implies a radio power limit of $\log P_{1.4\ GHz}$(W Hz^{-1}) = 20.74 at the distance of the Cancer cluster, the nearest in their sample ($z = 0.015$).

For a proper comparison we computed the b_J magnitude limit corresponding to the m_z limit in GB99. First we converted m_z in m_B according to the relationship $m_B = m_z - 0.35$ (Gaztañaga & Dalton, 2000), assuming $b_J \simeq m_B$ (Section 6.3). Then we applied a distance modulus of 1.5 mag and a 0.24 magnitude correction for the galactic absorption (Schlegel et al. 1998). We obtained a limit of $b'_J = 17.09$, where b'_J is the magnitude corrected as descibed above.

For each late–type radio galaxy in A3558–C we applied a correction for the internal extintion. This latter was determined according to Gavazzi & Boselli (1996) using an average value of 0.60 for the D_B(type) coefficient, which corresponds to Sb galaxies in the B band.

We selected, at the same radio power limit as GB99, a sample of spiral galaxies in A3558–C with $b'_J \leq 17.09$. The resulting sample includes 13 objects and is presented in Table 6. We remind that the radio powers in Table 6 are scaled to the cosmology adopted by GB99.

For each radio galaxy of our sample we computed the radio/optical ratio, defined in GB99 as R_B=$S_{1.4GHz}$ / k $\times\ 10^{-0.4\times b'_J}$, where k = 4.44×10^6 is the factor appropriate to transform in mJy the b_J magnitude. We note that this quantity is independent of distance. According to Gavazzi et al. (1996) R_B gives the ratio of the radio emission per unit light emitted by the relatively young stellar population. We compared the distribution of R_B ratios for the late–type galaxy sample in A3558–C to the subsample extracted from GB99 (Figure 8). We point out that the R_B distribution of our sample does not change significantly if we use coefficients D_B(type) corresponding to morphological types different from Sb.

The limited number of galaxies in A3558–C does not allow firm conclusions, however some considerations can be made. The most remarkable features in Fig. 8 are the peaked distribution (in the first bin) for the galaxies in poor environments, and the presence of galaxies (though a limited number) with a strong excess of radio emission both in rich and poor environments.
Considering poissonian errors in each bin, the distribution of radio late–type galaxies in A3558–C is substantially flat up to $R_B = 2$, similar to the distributions in Coma and A1367. We estimated the similarity between A3558–C and Coma applying a Kolmogoroff–Smirnov (KS) test to the two distributions and found that the probability that they are the same distribution is ∼92.4%. A KS test applied to A3558–C and the isolated galaxies gives a probability of only ∼3.6%.

The late–type galaxies with $R_B \gtrsim 4$ are missing in A3558–C (respectively 2/15 and 2/22 for A1367 and Coma), however this could be due to lack of statistics, since only 13 spirals in A3558–C are included in the analysis.

To summarise, the statistical properties of the radio emission from spiral galaxies in A3558–C are similar to those in rich and dynamically evolved environments.

8. Discussion and Conclusions

In this paper we presented deep 1.4 GHz VLA observations of the major cluster merger in the A3558 complex. The area under study, A3558–C, defined as the region between the centres of the two Abell clusters A3558 and A3562, including also the two groups SC 1329–213 and SC 1327–312, is thought to have recently experienced a major merger between two massive clusters. What we see now is expected to be the result of the first core–core encounter. The observational properties in this region, together with numerical simulations, suggest that A3558 is the main cluster, while the whole chain, beyond A3558 itself, is the remains of the colliding cluster (Bardelli et al. 2002).
A picture is emerging, in which radio AGN and starburst activity, radio relics and halos, or the lack thereof, are signature of cluster mergers at different stages. In particular, Venturi et al. (2002) proposed an evolutionary merger sequence to account for the diversity in the radio properties of the three main merging cluster systems in the core of the Shapley Concentration; Kempner & Sarazin (2001) postulated that radio halos and relics may form at different times during mergers; MO03 explained the different fraction of radio emitting galaxies (starburst and AGNs) in a cluster sample as due to different merger stages. With this study we have a unique opportunity to connect the observed properties in the radio band with a well defined cluster merger stage. This is of crucial importance for a better understanding of the complex effects of cluster mergers, with particular emphasis to the stage of

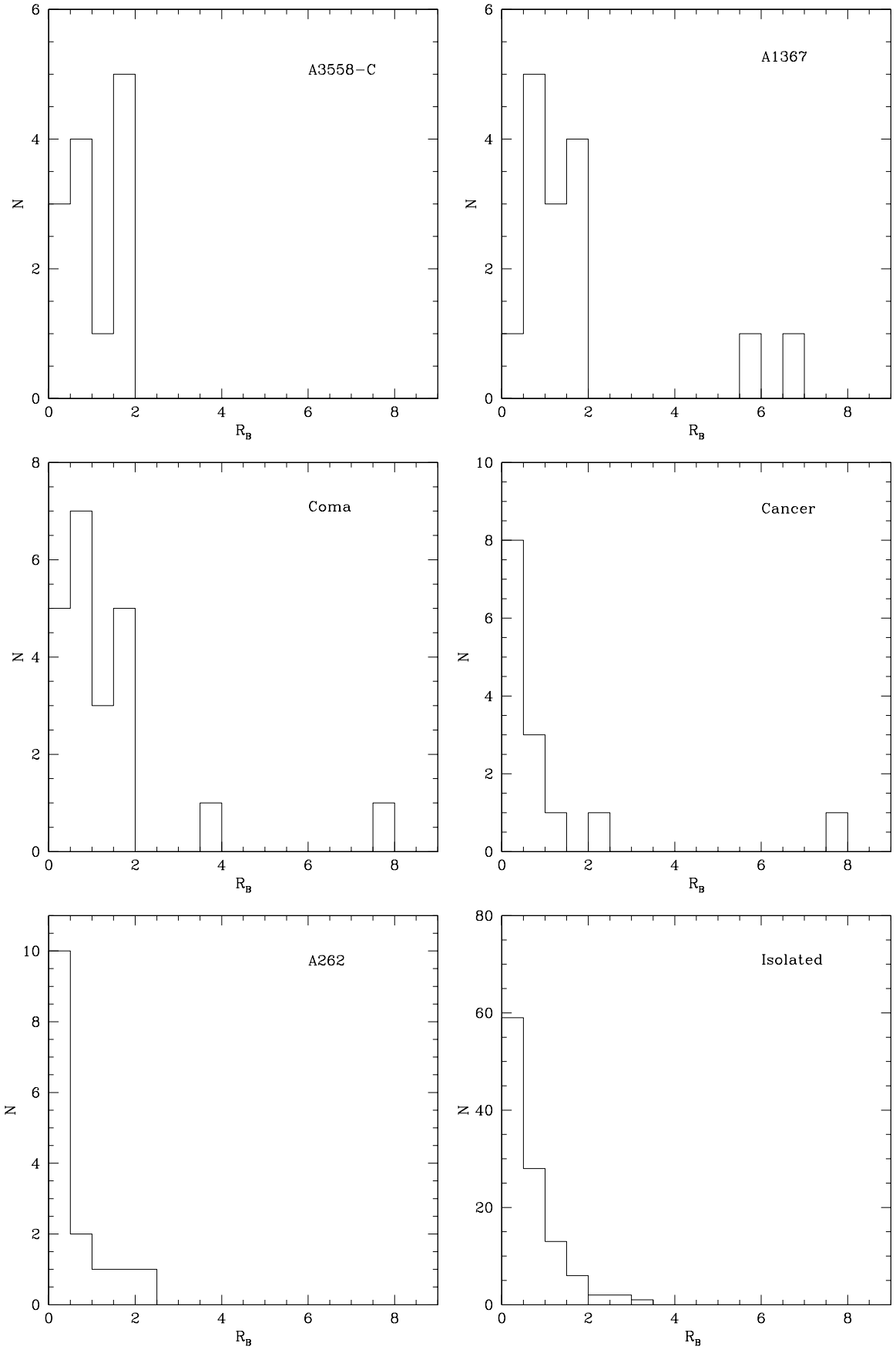

Fig. 8. Distributions of the R_B radio/optical ratios for the late–type galaxies in A3558–C, A1367, Coma, Cancer, A262 and for isolated galaxies in the Coma supercluster.

Table 6. Sample of late−type radio galaxies used for the RLF

Radio name	Optical name	b'_J	$S_{1.4GHz}$ mJy	$\log P_{1.4GHz}$ W Hz^{-1}	R_B
J1329−3119b	#10174	14.39	4.53	22.07	0.58
J1330−3124a	#10318	14.52	6.89	22.20	0.99
J1330−3113	#10313	16.42	1.79	21.76	1.49
J1330−3134	#10725	15.66	3.86	22.06	1.60
J1330−3143b	#10869	14.96	7.77	22.25	1.69
J1330−3209	#10888	15.91	0.73	21.17	0.38
J1331−3144	#11000	16.20	2.55	21.67	1.73
J1331−3113	#11243	14.88	2.38	21.83	0.48
J1331−3149b	#11751	16.61	1.82	21.58	1.81
J1332−3152a	#11753	15.67	0.49	21.04	0.20
J1333−3158	#12912	17.07	1.00	21.52	1.52
J1334−3141a	#13198	15.56	2.11	21.52	0.80
J1335−3133	#13629	15.52	2.21	21.69	0.80

the merger.
The most relevant results of our analysis can be summarised as follows:

(i) a faint radio halo is found at the centre of A3562, whose properties are consistent with the idea that it is a young source at the beginning of the reacceleration phase (V2003) induced by a recent merger event;
(ii) the origin of the extended emission in the radio galaxy J1332–3146a, associated with the dominant galaxy in the group SC 1329–313, is unclear. No radio jets are present in the nuclear region of J1332–3146a, and the nuclear radio component has steep spectrum. It is possible that this extended emission has actually cluster origins (see Section 6.2), being either (a) a "bright" area of a very low brightness bridge of radio emission, connecting A3562 and SC 1329–313, or (b) a "revived" radio emission region, where pre–existing old electrons were reaccelerated;
(iii) a large number of radio sources associated with A3558–C galaxies was found, i.e. 33 objects, most of them with radio emission at low power levels. Our analysis (see Section 6.3) suggests that 26/33 radio galaxies are candidate starbursts. Among them, 11 also show a blue excess;
(iv) the total number of radio AGNs detected in this region is consistent with the expectations from the RLF of LO96, suggesting that the cluster merger has not affected the probability of an early–type galaxy to develop a nuclear radio source;
(v) the distribution of the radio/optical ratios for the spirals in A3558–C is similar to what is found in rich and evolved environments.

The main question is if and how this wealth of observables is connected to the cluster merger in this region. Beyond the noticeable finding of the radio halo in the centre of A3562 (V2003), the radio properties of the Shapley galaxies in this region may contain important pieces of information.

V2000 showed that the RLF for early type galaxies in the whole A3558–C shows a deficit of radio galaxies compared to the "universal" RLF presented in LO96 (V2000), over the whole power range. On the other hand, the RLF for AGNs presented here matches the expectations of LO96; furthermore the outskirts of the chain (A3556 and A3562) contain the largest fraction of Shapley radio galaxies (see also Section 2). This suggests that A3558 itself, the most massive cluster in the chain, is the main responsible for the lack of radio sources in the RLF found in V2000. A possible explanation is the key role of A3558 in the merger, i.e. it is experiencing the most dramatic effects of the merger, being the result of the interaction of core regions of the two colliding clusters. If our interpretation is correct, then the role of cluster merger on the radio emission from AGNs may be many–fold, depending on the age and strength of the merger.
Optical photometric information on the faint population of radio galaxies in A3558–C confirms that at least 50% of these objects are most likely starburst candidates. However, a radio/optical analysis carried out following MO03 provides only weak evidence that the fraction of radio emitting galaxies in A3558–C is higher than in non–merging environments.
The statistical results on the late–type galaxies show that the radio emission in the A3558–C spirals is similar to those in rich and dynamically evolved clusters. This suggests that the radio emission in spiral galaxies may be one of the first "parameters" to react to a cluster merger event.

In conclusion, V2003 showed that the radio halo at the centre of A3562 is consistent with a reacceleration phase which started $\sim$ a few 10^8 years ago. This ongoing merger is therefore *advanced*, in the sense that the core–core encounter has already taken place, but it is still young if compared to the total duration expected for a cluster merger, i.e. 10^9 yr. Our study suggests that on this timescale, the effect of cluster merger on the radio emission from cluster galaxies is many–fold. In particular,

we found only marginal evidence of enhanced radio emission of starburst origin, but we found significant enhanced radio emission from spirals. We argue that the role of cluster merger on the nuclear activity in early–type galaxies is a complex phenomenon, since observational evidence in the whole A3558 cluster chain clearly shows that the deficit in radio galaxies found in V2000 is entirely due to the cluster A3558, which has experienced the most violent consequences of the merger.

Acknowledgements. This work has been partially supported by the Italian Space Agency grants ASI-I-R-105-00, ASI-I-R-037-01 and ASI-I-R-063-02, and by the Italian Ministery (MIUR) grant COFIN2001 "Clusters and groups of galaxies: the interplay between dark and baryonic matter". NRAO is a facility of the National Science Foundation, operated under cooperative agreement by Associated Universities, Inc.
This work has made use of the NASA/IPAC Extragalactic Database NED which is operated by the JPL, California Institute of Technology, under contract with the National Aeronautics and Space Administration.

Appendix A: Notes to optical identifications

− J1329−3122a : this radio source is the blend of two sources in the ATCA 22 cm catalogue: the pointlike J1329−3122, associated with a 18.54–mag galaxy, and the FRII J1329−3123, identified with the elliptical cluster galaxy #10178 (b_J = 19.08). The location of this latter is coincident with the radio emission peak of the 1.4 GHz VLA image, so we consider J1329−3122a associated to the elliptical cluster galaxy;
− J1330−3143b : this source is identified with the spiral #10869, but other two cluster galaxies fall within the radio isophotes of this extended source.
− J1330−3127 : this identification is uncertain since the candidate optical counterpart, which falls within the radio contours, is misplaced with respect to the radio emission peak.
− J1331−3139 : this source is the blend of the two J1331−3139a and J1331−3139b radio sources of the ATCA–22cm catalogue. The latter is identified with the 17.97–mag quasar.
− J1331−3143 : this source is probably the blend of more sources. A galaxy with $b_J = 16.82$ and z = 0.044 is located within the radio contours, at $\sim$ 45 arcsec from the radio emission peak.
− J1331−3155b: a spiral galaxy, with $b_J = 15.39$ and v = 4505 km s^{-1} is located at the edge of the radio contours, at $\sim$ 37 arcsec from the emission peak.
− J1332−3141a: a cluster galaxy with $b_J = 16.96$ and v = 10732 km s^{-1} lies within the radio contours of the source, at $\sim$ 50 arcsec from the emission peak.
− J1334−3132: this source is the blend of the three ATCA 22cm sources J1334−3132a, J1334−3132b e J1334−3132c. J1334−3132c is associated with the 17.30-mag elliptical galaxy #13281. This galaxy falls within the radio contours of the 1.4 GHz VLA image, but it is dislocated with respect to the emission peak.

References

Abell G.O., Corwin H.G., Olowin R.P. 1989, A&AS, 70, 1 (ACO)
Balogh M.L., Schade D., Morris S.L., Yee H.K.C., Carlberg R.G., Ellingson E. 1998, ApJ, 504, L75
Bardelli S., Zucca E., Vettolani G., et al. 1994, MNRAS, 267, 665
Bardelli S., Zucca E., Malizia A., et al. 1996, A&A, 305, 435
Bardelli S., Pisani A., Ramella M., Zucca E., Zamorani G. 1998a, MNRAS, 300, 589
Bardelli S., Zucca E., Zamorani G., Vettolani G., Scaramella R. 1998b, MNRAS, 296, 599
Bardelli S., Zucca, E., Zamorani, G., Moscardini, L., Scaramella, R., 2000, MNRAS, 312, 540
Bardelli S., De Grandi S., Ettori S., Molendi S., Zucca E., Colafrancesco S. 2002, A&A, 382, 17
Bekki K. 1999, ApJ, 510, L15
Bothun G., Dressler A. 1986, ApJ, 301, 57
Breen J., Raychaudhury S., Forman J., Jones C. 1994, ApJ, 424, 59
Burns J.O., Roettiger K., Ledlow M., Klypin A. 1994, ApJ, 427, L87
Condon, J.J., Cotton, W.D., Broderick, J.J., 2002, AJ, 124, 675
de Ruiter H.R., Willis, A.G., Arp, H.C., 1977, A&AS, 28, 211
Dwarakanath, K.S., Owen, F.N. 1999, AJ, 118, 625
Ettori S., Fabian A.C., White D.A. 1997, MNRAS, 289, 787
Ettori S., Bardelli S., De Grandi S., Molendi S., Zamorani G., Zucca E. 2000, MNRAS, 318, 239
Fujita Y., Tazikawa M., Nagashima M., Enoki M. 1999, PASJ, 51, L1
Fukugita M., Shimasaku K., Ichikawa T. 1995, PASP, 107, 945
Gaztañaga E., Dalton G.B. 2000, MNRAS, 312, 417
Gavazzi G., Jaffe W. 1986, ApJ, 310, 53
Gavazzi G., Boselli A. 1996, Astroph. Lett. & Commun., 35, 1
Gavazzi G., Boselli A. 1999, A&A, 343, 93 (GB99)
Gunn J.E., Gott J.R. 1972, ApJ, 176, 1
Hambly, N. C., MacGillivray, H. T., Read, M. A., Tritton, S. B., Thomson, E. B., Kelly, B. D., Morgan, D. H., Smith, R. E., Driver, S. P., Williamson, J., Parker, Q. A., Hawkins, M. R. S., Williams, P. M., Lawrence, A. 2001, MNRAS, 326, 1279
Jaffe W., Perola G.C. 1976, A&A, 46, 275
Kempner, J.C, Sarazin, C.L. 2001, ApJ, 548, 639
Ledlow M.J., Owen F.N. 1996, ApJ, 112, 9 (LO96)
Lumsden S.L., Collins C.A., Nichol R.C., Eke V.R., Guzzo L. 1997, MNRAS, 290, 119
Maddox S.J., Efstathiou G., Sutherland W.J., Loveday J. 1990, MNRAS, 243, 692
Metcalfe N., Godwin J.G., Peach J.V. 1994, MNRAS, 267, 431
Miller, N.A., Owen, F.N., Hill, J.M. 2003, AJ, 125, 2393
Miller, N.A., Owen, F.N. 2003, AJ, 125, 2427 (MO03)
Owen F.M., Ledlow M.J., Keel W.C., Morrison G.E. 1999, AJ, 118, 633
Prandoni I., Gregorini L., Parma P., de Ruiter H.R., Vettolani G., Wieringa M.H., Ekers R.D. 2000, A&A Suppl. Ser., 146, 41
Prandoni I., Gregorini L., Parma P., de Ruiter H.R., Vettolani G., Wieringa M.H., Ekers R.D. 2001, A&A, 365, 392
Roettiger K., Loken C., Burns J.O. 1997, ApJS, 109, 307
Schlegel D.J., Finkbeiner D.P., Davis M. 1998, ApJ, 500, 525
Unewisse A.M., Hunstead D.W., Pietrzynski B. 1993, Pubbl. Astron. Soc. Austr., 10, 229

Venturi, T., Bardelli, S., Morganti, R., Hunstead, R.W. 1997, MNRAS, 285, 898
Venturi, T., Bardelli, S., Morganti, R., Hunstead, R.W. 1998, MNRAS, 298, 1113
Venturi T., Bardelli S., Morganti R., Hunstead R.W. 2000, MNRAS, 314, 594 (V2000)
Venturi T., Bardelli S., Zambelli G., Morganti R., Hunstead R.W. 2001, MNRAS, 324, 1131
Venturi, T., Bardelli, S., Zagaria, M., Prandoni, I., Morganti, R. 2002, A&A, 385, 39
Venturi T., Bardelli S., Dallacasa D., Brunetti G., Giacintucci S., Hunstead R.W., Morganti R. 2003, A&A, 402, 913 (V2003)
Vettolani G., Zucca E., Zamorani G., Cappi A., Merighi R., Mignoli M., Stirpe G.M., MacGillivray H., Collins C., Balkowski C., Cayatte V., Maurogordato S., Proust D., Chincarini G., Guzzo L., Maccagni D., Scaramella R., Blanchard A., Ramella M. 1997, A&A, 325, 954
Vollmer B., Braine J., Balkowski C., Cayatte V., Duschl W.J. 2001, A&A, 374, 824
Yentis D.J., Cruddace R.G., Gursky H., Stuart B.V., Wallin J.F., MacGillivray H.T., Collins C.A. 1992, in Digitised Optical Sky Surveys, Editors, H.T. MacGillivray, E.B. Thomson; Publisher, Kluwer Academic Publishers, p.67
Yun, M.S., Reddy, N.A., Condon, J.J. 2001, ApJ, 554, 803